2014

Tracing Inflows and Outlflows with Absorption Lines in Circumgalactic Gas

Amanda Brady Ford
Romeel Dave
Benjamin D. Oppenheimer
Neal S. Katz, *University of Massachusetts - Amherst*
Juna A. Kollmeier, et al.

Tracing Inflows and Outflows with Absorption Lines in Circumgalactic Gas

Amanda Brady Ford[1], Romeel Davé[2,3,4,1], Benjamin D. Oppenheimer[5,6], Neal Katz[6], Juna A. Kollmeier[7], Robert Thompson[1], David H. Weinberg[8]

[1] *Astronomy Department, University of Arizona, Tucson, AZ 85721, USA*
[2] *University of the Western Cape, Bellville, Cape Town 7535, South Africa*
[3] *South African Astronomical Observatories, Observatory, Cape Town 7925, South Africa*
[4] *African Institute for Mathematical Sciences, Muizenberg, Cape Town 7945, South Africa*
[5] *Leiden Observatory, Leiden University, PO Box 9513, 2300 RA Leiden, Netherlands*
[6] *CASA, Department of Astrophysical and Planetary Sciences, University of Colorado, Boulder, CO 80309, USA*
[7] *Astronomy Department, University of Massachusetts, Amherst, MA 01003, USA*
[8] *Observatories of the Carnegie Institution of Washington, Pasadena, CA 91101, USA*
[9] *Astronomy Department and CCAPP, Ohio State University, Columbus, OH 43210, USA*

15 October 2013

ABSTRACT

We examine how HI and metal absorption lines within low-redshift galaxy halos trace the dynamical state of circumgalactic gas, using cosmological hydrodynamic simulations that include a well-vetted heuristic model for galactic outflows. We categorize inflowing, outflowing, and ambient gas based on its history and fate as tracked in our simulation. Following our earlier work showing that the ionisation level of absorbers was a primary factor in determining the physical conditions of absorbing gas, we show here that it is also a governing factor for its dynamical state. Low-ionisation metal absorbers (e.g. Mg II) tend to arise in gas that will fall onto galaxies within several Gyr, while high-ionisation metal absorbers (e.g. O VI) generally trace material that was deposited by outflows many Gyr ago. Inflowing gas is dominated by enriched material that was previously ejected in an outflow, hence accretion at low redshifts is typically substantially enriched. Recycling wind material is preferentially found closer to galaxies, and is more dominant in lower-mass halos since high-mass halos have more hot gas that is able to support itself against infall. Low-mass halos also tend to re-eject more of their accreted material, owing to our outflow prescription that employs higher mass loading factors for lower-mass galaxies. Typical HI absorbers trace unenriched ambient material that is not participating in the baryon cycle, but stronger HI absorbers arise in cool, enriched inflowing gas. Instantaneous radial velocity measures of absorbers are generally poor at distinguishing between inflowing and outflowing gas, except in the case of very recent outflows. These results suggest that probing halo gas using a range of absorbers can provide detailed information about the amount and physical conditions of material that is participating in the baryon cycle.

1 INTRO

The modern view of galaxy formation relies on continual inflows of gas from the intergalactic medium (e.g. Kereš et al. 2005; Brooks et al. 2009; Dekel et al. 2009; Bouché et al. 2010; Davé et al. 2012; van de Voort et al. 2012), counteracted by strong galactic-scale outflows (e.g. Oppenheimer et al. 2010; Davé et al. 2011a), which in concert establish the growth rate of gas and stars within galaxies at all cosmic epochs. This "baryon cycle" view of galaxy formation has alleviated many of the classic problems in galaxy formation such as overcooling (e.g. White & Frenk 1991; Balogh et al. 2001; Springel & Hernquist 2003) and the formation of overly compact disk galaxies (e.g. Governato et al. 2007; Brook et al. 2012). The amount of ejected material in these types of models is typically comparable to or exceeds the

star formation rate (e.g. Oppenheimer & Davé 2008), and thus the inflow rate is expected to be several to many times the star formation rate.

Despite the large amounts of mass purportedly moving in and out of galaxies, direct comparison between observations and theoretical predictions remain difficult. Outflows are seen emanating from low (e.g. Martin 2005; Rupke et al. 2005; Tremonti et al. 2007), intermediate (e.g. Weiner 2009; Rubin et al. 2012) and high (e.g. Pettini et al. 2001; Steidel 2001; Veilleux et al. 2005) redshift star-forming galaxies, but the amount of mass involved is difficult to estimate directly (e.g. Genzel et al. 2010; Martin et al. 2013) owing to complex ionisation conditions and the tenuous, multiphase nature of the outflowing material. Inflows, meanwhile, are even more difficult to detect, and there are only tan-

talising hints from redshifted IGM absorption lines (Rubin et al. 2012), though it has been argued that Lyman-alpha blobs (Goerdt et al. 2010), Lyman limit absorption systems (e.g. Fumagalli et al. 2011; Lehner et al. 2012), low metallicity gas (Lehner et al. 2013) and high column density H I systems (van de Voort et al. 2012) may be indirect markers of such accretion, and Faucher-Giguère & Kereš (2011) argue that cold accretion streams would have very low covering fractions. Nonetheless, simple arguments from observed galaxy properties such as the gas-phase metallicity (e.g. Erb et al. 2006) and the evolution of the gas content (Tacconi et al. 2010) strongly suggest that inflows and outflows must be occurring. Clearly, a better understanding of the physical processes involved is crucial for establishing a complete view of how galaxies evolve across cosmic time. This paper examines the dynamics and origin of accreting and outflowing gas in a cosmological hydrodynamic simulation, at redshift z=0.25, and discusses absorption-line diagnostics that can trace these components.

A separate aspect of cosmic baryons influenced by galactic outflows is the metal content of the intergalactic medium (IGM). Intergalactic metals are seen in quasar absorption line spectra from almost the earliest epochs where such data can be obtained (e.g. Songaila 2001; Becker et al. 2011; Simcoe et al. 2011), as well as at lower redshift (e.g. Tripp et al. 2000, 2008; Thom & Chen 2008; D'Odorico et al. 2010; Tumlinson et al. 2011; Cooksey et al. 2013; Tilton et al. 2012; Werk et al. 2013), indicative of enrichment by strong galactic outflows (Aguirre et al. 2001b; Oppenheimer & Davé 2006). IGM enrichment observations can thus place tight constraints on the properties of outflows (Oppenheimer & Davé 2006; Wiersma et al. 2010; Oppenheimer et al. 2012). However, the enrichment observed far from galaxies may only track the ancient relics of outflows, rather than the actively ongoing baryon cycle. Also, such metal lines may not trace inflows effectively if the accreting material is metal-poor.

Recently, much attention has been focused on the circumgalactic medium (CGM), a loosely-defined term that can alternately mean the gas within some fixed distance of a galaxy (e.g. Rudie et al. 2012; Ford et al. 2013), within the typical metal-enriched region around a galaxy (e.g. Prochaska et al. 2013), or within the virial radius of the galaxy's dark matter halo (Stocke et al. 2013). The CGM is where the baryon cycle is expected to be in action, where material is both flowing into galaxies to fuel star formation, and being expelled from galaxies on its journey into the IGM. Hence a potentially powerful tool to explore the baryon cycle is to examine inflowing and outflowing gas in the CGM, either in emission or, as we discuss here, in absorption against background sources whose lines of sight pass through a galaxy's CGM.

The recent installation of the Cosmic Origins Spectrograph aboard *Hubble* has enabled the CGM to be probed in absorption in unprecedented detail. As an example, the COS-Halos project (Tumlinson et al. 2011, 2013) examines the CGM around more than 70 galaxies spanning a range in mass and colour, providing a comprehensive look at the CGM within ∼150 kpc of galaxies ranging in size from L^* to Magellanic-sized dwarfs (Werk et al. 2013). Other studies have targeted randomly situated bright quasars but have obtained extensive galaxy redshift information along their lines of sight, and are thus able to probe the CGM out to several hundred kpc (e.g. Tripp et al. 2006; Stocke et al. 2013). The Mg II doublet, which redshifts into the optical at $z \gtrsim 0.2$, has long been used as a probe of CGM gas (Churchill et al. 2000; Bordoloi et al. 2011; Chen 2012; Kacprzak et al. 2012) out to many tens of kpc. These studies have already highlighted some interesting results, including the fact that the presence of O VI is highly correlated with specific star formation rate (Tumlinson et al. 2011), but the presence of low-ionisation lines such as strong HI (Thom et al. 2012), Mg II (Chen 2012), and Si III (Werk et al. 2013) is not.

One would like to assemble the multitude of observed absorption features, from HI to low-ionisation IGM metal lines, to high-ionisation lines that presumably trace more diffuse or hotter gas, into a coherent picture for how the baryon cycle operates. To properly place these data within a cosmological context, interpretive models must be cosmological in nature, and they must explicitly include galactic outflows and properly account for inflows. However, modelling the detailed physics of the interaction between inflowing, outflowing, and ambient gas remains a great challenge. Inflows are thought to be filamentary but some simulations predict highly collimated and cold filaments (e.g. Dekel et al. 2009), others suggest more diffuse, warmer filaments (e.g. Torrey et al. 2013), while still others suggest that filaments may break up via thermal instabilities depending on the environment (Kereš & Hernquist 2009). Outflows also have large modelling uncertainties, as the way in which outflows are powered is still not fundamentally understood, and different approaches can lead to different results regarding the nature of the CGM gas and its absorption signatures (Stinson et al. 2012; Hummels et al. 2013; Ford et al. 2013). Finally, it is possible that conductive interfaces on cold clouds moving through the CGM may be responsible for high-ionisation metal lines such as O VI and Ne VIII in particular (e.g. Tripp et al. 2011), and such interfaces would be well beyond the ability for any current cosmological simulation to resolve. Hence, these are early days in understanding how to interpret CGM absorption data, and much work remains. Nonetheless, some basic characteristics of the CGM and its relation to the baryon cycle are likely to be robust in such models.

In this series of papers, we explore the physical conditions and observable properties of the CGM using smoothed particle hydrodynamics (SPH)-based cosmological simulations. In Ford et al. (2013), we examined the general physical properties of the CGM, as well as absorption statistics as a function of impact parameter, for HI, Mg II, Si IV, C IV, O VI, and Ne VIII. In our simulations, the physical conditions traced by any given ion are often a monotonic function of its ionisation potential, such that low ionisation potential ions (which we will call low ions) generally trace high-density gas very close to galaxies at photo-ionisation temperatures (around 10^4K), higher ionisation potential ions (which we will call high ions) trace increasingly more diffuse, lower-density gas, and the highest ions can trace hot gas when present (typically in halos with masses $\gtrsim 10^{12} M_\odot$). We presented predictions for the integrated column density and column density distributions for these absorbers, as a function of impact parameter, and showed that low ion absorbers increase in strength dramatically when lines of sight pass close to galaxies, while higher ions show a more modest increase

closer to galaxies. These trends can be tested quantitatively against current and forthcoming observations; comparisons that we are conducting now and will present in future work.

In this paper, we continue our focus on the physical state of the CGM by examining the dynamical state of the CGM gas and its impact on observable absorption line properties. In particular, we ask the question: Can we distinguish inflowing, outflowing, and ambient gas based on CGM absorption signatures? Here we focus on examining this at low redshifts ($z \sim 0 - 0.25$), in anticipation of exploring the constraints on models enabled by COS-Halos and similar CGM projects; we leave an examination of this question at high redshifts for future work.

To explore the dynamical state of CGM baryons, we implement an analysis scheme that tracks gas as it moves in and out of galaxies. Such tracking, we note, is uniquely enabled by our particle-based simulation methodology. By tracking exactly where the gas originates and where it will eventually reside, we can definitively identify which gas is inflowing, outflowing, and ambient over a certain timescale. Moreover, this enables us to track material that once flowed out of a galaxy but that will eventually return to a galaxy, a process we call *wind recycling* (Oppenheimer et al. 2010). This component has key observational implications becase it represents inflowing material that is enriched and hence can be traced in metal absorption. Indeed, we will show (as in Oppenheimer et al. 2010) that wind recycling provides a dominant inflow contribution at the present cosmic epoch, which is by default lacking in models that do not include outflows. We will further show that absorption from low ions typically comes from recycling inflows, while absorption from high ions comes mostly from ancient outflows.

We organise our paper as follows: in §2 we introduce our simulations and methods, in §3 we define and explore various categories of inflowing, outflowing, and ambient material, and in §4 we present observational diagnostics to distinguish among these categories. In §5 we examine the physical conditions of these categories, in §6 we discuss numerical considerations in our (and alternate) simulation methods, and in §7 we present our conclusions.

2　SIMULATIONS & ANALYSIS

2.1　The Code and Input Physics

We use our modified version (Oppenheimer & Davé 2008) of the N-body+entropy-conserving smooth particle hydrodynamic (EC-SPH) code GADGET-2 (Springel 2005), which is more fully described in §2.1 of Davé et al. (2010). Our main simulation for this work is identical to that in Davé et al. (2013), and we refer the reader to that work for a more detailed description.

We assume a ΛCDM cosmology (Hinshaw et al. 2009): $\Omega_M = 0.28$, $\Omega_\Lambda = 0.72$, $h = \mathrm{H}_o/(100\ \mathrm{km\,s}^{-1} Mpc^{-1}) = 0.7$, a primordial power spectra index $n = 0.96$, an amplitude of the mass fluctuations scaled to $\sigma_8 = 0.82$, and $\Omega_b = 0.046$. We use a cubic volume of $32h^{-1}$ Mpc on a side with 512^3 dark matter and 512^3 gas particles, and a softening length of $\eta = 1.25h^{-1}$ kpc (comoving, Plummer equivalent). The gas particle mass is $4.5 \times 10^6 M_\odot$; dark matter particle mass is $2.3 \times 10^7 M_\odot$. The stellar component of a Milky Way mass galaxy is thus represented with $\approx 2 \times 10^4$ particles.

We incorporate cooling processes using primordial abundances as described by Katz et al. (1996), with metal line cooling based on tables from Wiersma et al. (2009a) that assume ionisation equilibrium in the presence of the Haardt & Madau (2001) background. Star formation follows a Schmidt (1959) Law calibrated to the Kennicutt (1998) relation, following Springel & Hernquist (2003). The ISM is modelled using the sub-grid recipe of Springel & Hernquist (2003), where a gas particle above a density threshold of $n_H = 0.13$ cm^{-3} is modelled as a fraction of cold clouds embedded in a warm ionised medium following McKee & Ostriker (1977). We use the Chabrier (2003) initial mass function (IMF) throughout. We account for metal enrichment from Type II supernovae, Type Ia SNe, and AGB stars, and we track four elements (C,O,Si,Fe) individually, as described in more detail in Oppenheimer & Davé (2008).

This simulation includes galactic outflows, which are implemented using a Monte Carlo approach. These outflows are tied to the SFR, $\dot{M}_{wind} = \eta \times SFR$, where η is the mass loading factor. For this work we focus on the hybrid energy/momentum driven winds, or "ezw" model. In the ezw model, the wind speed and mass loading factor depend on the galaxy velocity dispersion σ:

$$v_\mathrm{w} = 3\sigma\sqrt{\mathrm{f}_L - 1} \tag{1}$$

$$\eta = \sigma_o/\sigma,\ \mathrm{if}\ \sigma > 75\ \mathrm{km\,s}^{-1} \tag{2}$$

$$\eta = (\sigma_o/\sigma)^2,\ \mathrm{if}\ \sigma < 75\ \mathrm{km\,s}^{-1} \tag{3}$$

where f_L is the luminosity in units of the Eddington luminosity required to expel gas from a galaxy potential, $\sigma_o = 150$ km s^{-1}, and σ is the galaxy's internal velocity dispersion (Oppenheimer & Davé 2008).

These scalings roughly capture the behaviour in recent models of outflows from the interstellar medium by Murray et al. (2010) and Hopkins et al. (2012). We note that the scalings for this "ezw" model, and those in previous work by our group with the momentum-driven or "vzw" model (e.g. Oppenheimer & Davé 2008; Davé et al. 2010, 2011a,b; Oppenheimer et al. 2012; Ford et al. 2013), which follow the scalings of Murray et al. (2005) are identical for higher mass systems. It is only in lower mass systems, i.e. those with $\sigma < 75$ km s^{-1}, where the ezw model differs from the vzw model. In this particular simulation, we also add an artificial quenching mechanism in higher mass halos, as described by Davé et al. (2013).

2.2　Generating spectra with SPECEXBIN

We use SPECEXBIN, described in more detail by Oppenheimer & Davé (2006), to calculate the physical properties of the gas. SPECEXBIN averages physical properties of the gas along a given sight line, then uses look-up tables calculated with CLOUDY (Ferland et al. 1998, version 08.00) to find the ionisation fraction for the relevant ionic species. We use the same version of SPECEXBIN as in Ford et al. (2013), which includes a prescription for self-shielding from the ionisation background. This prescription results in a density threshold of approximately 0.01 cm^{-3} above which H I is fully neutral and moves all the magnesium into Mg II. See Figure 1 of Ford et al. (2013) for an example of a simulated spectrum.

We fit Voigt profiles to the absorption features using AUTOVP (Davé et al. 1997). As in Ford et al. (2013), we consider all components within $\pm$ 300 $\mathrm{km\,s^{-1}}$ to be associated with a galaxy, and we combine any components into systems with $\Delta v < 100\ \mathrm{km\,s^{-1}}$. We apply the same column density limits as in Ford et al. (2013), $10^{16}\ \mathrm{cm^{-2}}$ for H I and $10^{15}\ \mathrm{cm^{-2}}$ for metal lines. All lines stronger than this are set to this value to avoid having a single large saturated absorber skew the results, since such high column absorbers generally have highly uncertain column densities from Voigt profile fitting. As we showed in Ford et al. (2013), very weak lines are also poorly constrained given our assumed S/N=30, so we do not consider lines weaker than 30 mÅ.

For this work, we focus on targeted lines of sight (LOS). We randomly select central galaxies in two different halo mass bins: $10^{10.75-11.25}$ M$_\odot$ (labelled 10^{11} M$_\odot$) and $10^{11.75-12.25}$ M$_\odot$ (labelled 10^{12} M$_\odot$). For $10^{11}M_\odot$, we select 250 galaxies, while for $10^{12}M_\odot$ there are only 221 central galaxies in the simulation so we use all of them in our sample. We choose impact parameters ranging from 10 kpc out to 300 kpc, with the spacing increasing slightly with impact parameter. As in Ford et al. (2013) we produce four LOS per galaxy at a position x, y: x+b, x-b, y+b, y-b, for a total of 1,000 LOS per b per mass bin (844 for $10^{12}M_\odot$). We do not present results within 10 kpc of galaxies since we cannot resolve the detailed internal structure of the interstellar medium (ISM), and in any case we are more interested in probing CGM gas in absorption towards background objects that rarely lie at such small impact parameters. For parts of this work we restrict our study to gas within the virial radius of a central galaxy. We define the virial radius as the radius enclosing the virialization overdensity for our assumed cosmology, as described in (Davé et al. 2010, see their eqs. 1 and 2), which at $z = 0.25$ corresponds to roughly 90 times the critical density. The median central galaxy stellar mass is 5.89×10^8 and 3.63×10^{10} $M_\odot$ for our $10^{11}M_\odot$ and $10^{12}M_\odot$ halos, respectively.

We look at H I, Mg II, Si IV, C IV, O VI, and Ne VIII Ford et al. (2013). We select these ions as they are some of the most commonly observed species in the low-redshift CGM, spanning a wide range of ionisation potentials. All the metal lines have doublets, making their identification in observed spectra more straightforward.

3   INFLOWS AND OUTFLOWS

3.1   Identifying Inflowing and Outflowing Gas

To examine the dynamical state of CGM gas, we must first determine whether a given gas particle is inflowing, outflowing, or ambient. This is not trivial, because the constant cycling of baryons within halos can conflate inflowing, outflowing, and ambient gas.

Our approach is to make these divisions based on information available in the simulations: the particles' past history and future fate. For this, we require two additional pieces of information from the simulations: The future location of particles, and the time when each wind particle was ejected.

The first piece of information is the particles' future location. For this, we cross-correlate all the non-ISM particles in our simulation at $z = 0.25$ with their location at

$z = 0$, which is 3 Gyr later. If during this time a particle has been accreted into the ISM of a galaxy, or has turned into a star, or has been cycled through the ISM and subsequently ejected in an outflow, we identify it as an "accreting" particle. *Accretion is thus defined as any gas that was not in the ISM at $z = 0.25$, but is either in or has passed through the ISM or has turned into a star by $z = 0$.* By definition, the ISM consists of all gas with $n_H \geqslant 0.13\ \mathrm{cm^{-3}}$, the density threshold at which star formation is allowed.

Next, we need the time of ejection for each wind particle. We record each wind ejection event during the simulation so that for any given time we can determine the *wind age* of a given particle. If a particle *is not accreting* but has a non-zero wind age, it is considered an "outflow" particle. Note that the wind age can be quite large if a particle was ejected in the early universe, and hence being an outflow particle under this definition does not necessarily imply that it is currently on its way out from a galaxy. For particles ejected multiple times, we only record the most recent ejection. Finally, we define "ambient" gas as particles that will not accrete by $z = 0$ and was never ejected in a wind before $z = 0.25$. Thus we have the following divisions:

(i) **Pristine Accretion**. This is any accreting gas that has never been ejected in a wind. In general, this gas tends to have quite low metallicity since it has never been in the ISM of a galaxy. It can have non-zero metallicity, however, due to enrichment from tidal stripping or in-situ star formation at an earlier epoch.

(ii) **Recycled Accretion**. This is all accreting gas that was once ejected in a wind at least once before $z = 0.25$.

(iii) **Young Outflows**. These are gas particles that are not in the ISM at $z = 0.25$, are not accreting, and have been ejected from the galaxy in a wind between 0 and 1 Gyr before $z = 0.25$. We choose 1 Gyr as this is roughly the time a particle would take to leave the halo if it simply got kicked into the a wind, never scattered or slowed down due to forces other than gravity. For our cosmology, 1 Gyr before $z = 0.25$ is approximately $z = 0.36$.

(iv) **Ancient Outflows**. Same as young outflows, only particles ejected more than 1 Gyr ago (before $z = 0.36$).

(v) **Ambient**. Gas particles that are not in the ISM of a galaxy at $z = 0.25$, are not going to accrete onto a galaxy by $z = 0$ and that have never been in a wind by $z = 0$.

All gas particles that are not in the ISM at z=0.25 are in one of these five categories. Note, in particular, that the distinction between outflow (AO and YO) material and recycled accretion material, and the distinction between ambient (AMB) material and pristine accretion (PA), is whether the gas will accrete by $z = 0$.

Note that young and ancient outflows are subdivided by time since ejection, but in general ancient outflows end up farther away from galaxies, while outflows ejected more recently tend to stay closer. This reflects the "outside-in" IGM enrichment scenario occurring in our simulations as described in Oppenheimer et al. (2012). Also, recycled accretion can in principle escape the halo before re-accreting.
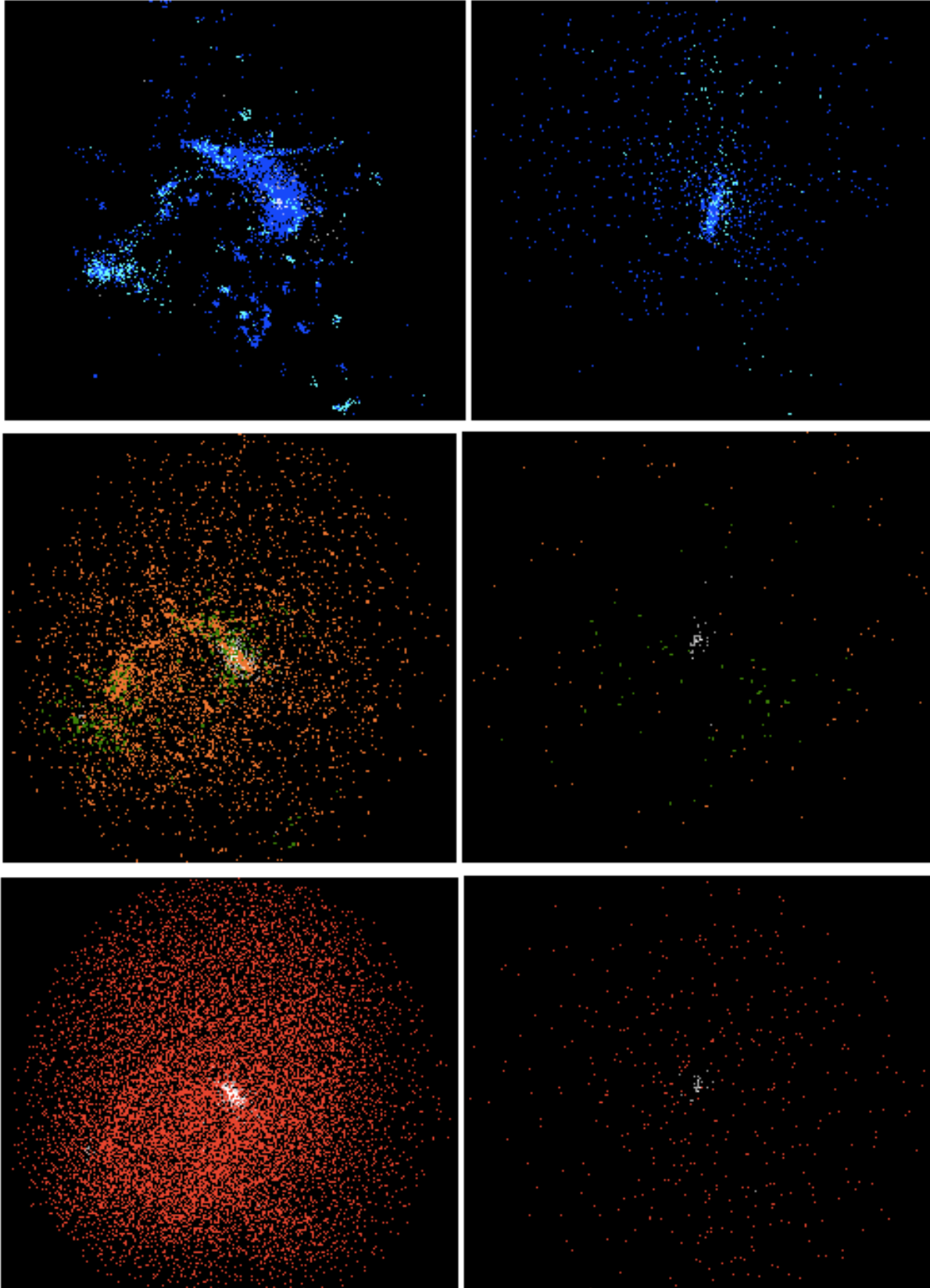
Figure 1. Left panels: SPH particles around a galaxy with halo mass $M_{halo} = 10^{12} M_{\odot}$ and a panel width of 525 physical kpc. Right panels: SPH particles around a galaxy with halo mass $M_{halo} = 10^{11} M_{\odot}$, panel width is 225 kpc. Top panels show recycled accretion (dark blue), and pristine accretion (light blue). Middle panels show young outflows (green) and ancient outflows (orange). Lower panels show ambient gas (red). All panels also include stars (white).

We visualise these categories in Figure 1, which shows a typical galaxy in a $10^{12} M_\odot$ halo (left panels) and in a $10^{11} M_\odot$ halo (right panels). We plot all the gas within the virial radius, 262 physical kpc for the $10^{12} M_\odot$ halo and 112 physical kpc for the $10^{11} M_\odot$ halo. Both galaxies are shown approximately edge-on. In each panel we plot the stars in white. In the top panels we plot the accreting material with recycled accretion in dark blue and pristine accretion in light blue. In the middle panels we plot recent outflows in green and ancient outflows in orange. In the lower panels we plot the ambient gas in red.

These images reveal some qualitative trends regarding these categories. Let us first examine the geometry. One may expect accreting material to flow in along the filaments, parallel to the disk of the galaxy, and outflowing material to come out perpendicular to the plane of the disk. However, the real picture is not so simple. First, only pristine accretion is expected to be along the filaments while recycled accretion, having been ejected from a galaxy, tends to be less confined to filaments. Second, the filaments and disks are not always aligned (Danovich et al. 2012), so even pristine material flowing in along a filament may not be parallel to the galaxy. For both masses in Figure 1, neither recycled nor pristine accretion is clearly coming in along a well-defined axis. For the $10^{12} M_\odot$ halo, the recycled accretion appears to follow some sort of structure while for the $10^{11} M_\odot$ halo it is more diffuse.

Moving to the middle panels we see that in the $10^{12} M_\odot$ case the young outflows generally are close to the main galaxy, its satellite, or the bridge that connects them. In the $10^{11} M_\odot$ case they are more diffuse. Interestingly, in neither the $10^{12} M_\odot$ or $10^{11} M_\odot$ case do the young outflows show an obvious polar axis preference, as one might have expected, despite the fact that the material is ejected in the direction of $\mathbf{v} \times \mathbf{a}$. In part this is because our "young" outflows are not that young, and in many cases may already be rejoining the accretion flow as recycled winds. For both masses ancient outflows are diffusely distributed. The ambient gas in the bottom panel fills the halo roughly spherically, without a preferred direction. We will show that much of the ambient material is in a hot hydrostatic gaseous halo, which is much more prominent at $10^{12} M_\odot$ than at $10^{11} M_\odot$ (Kereš et al. 2005; Gabor & Davé 2012).

To visualise these categories more quantitatively, in Figure 2 we show the wind age versus the $z = 0$ overdensity of all non-ISM gas particles (at $z = 0.25$) that have ever been ejected in an outflow. The vertical line demarcates the ISM overdensity threshold at $z = 0$, i.e. $n_H = 0.13$ cm^{-3}. Particles with densities greater than the ISM threshold at $z = 0$ are considered to be recycled accretion. Particles that are not in the ISM at $z = 0$ are subdivided by their wind age into ancient outflows (wind age > 1 Gyr) and young outflows (wind age $\leqslant$ 1 Gyr). The other two categories, pristine accretion and ambient, do not appear in this plot since they have never been in a wind by definition. This figure shows not just how we have divided our categories but also the distribution of the gas particles. One can see there are more particles in the ancient outflow category than in young outflows, and that the number of particles in the recycled accretion category is large. We will quantify this in greater detail in later sections.

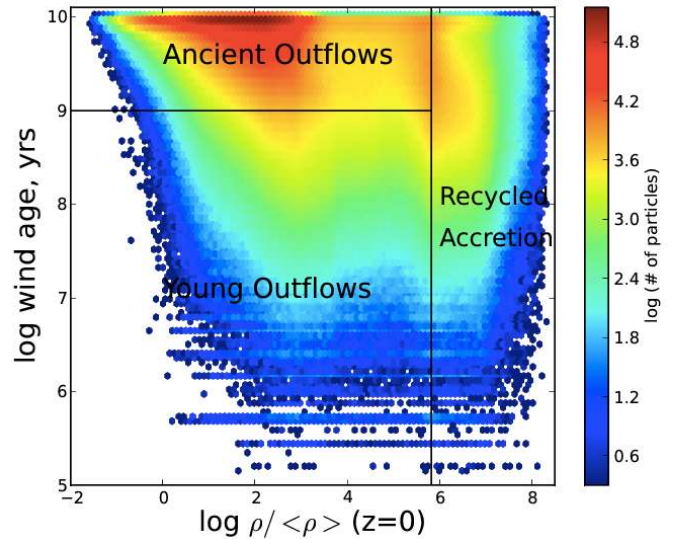We emphasise that we do not *just* look at the $z = 0$

Figure 2. The time (relative to $z = 0.25$) since last wind ejection vs. density at $z = 0$ of all gas not in the ISM at $z = 0.25$. The vertical line denotes ISM densities at $z = 0$. Gas to the right of the line is defined as accreting, because it will join the ISM of a galaxy by $z = 0$. Gas to the left is defined as not accreting, unless it forms a star or gets launched into a wind (not shown on this plot). The horizontal line at 9.0 shows the separation of young from ancient outflows.

Table 1. Fate of the accreting material

log(Halo Mass)	Star	Wind Ejection	ISM
11.0	10%	18%	72%
11.5	23%	30%	47%
12.0	31%	35%	34%

ISM densities (as shown in Figure 2) to determine whether or not a particle will accrete by $z = 0$. As we explained earlier, if a particle turns into a star or enters the galaxy and is subsequently ejected we also consider that particle as being accreted. In Table 1 we show, in three halo mass bins, what fraction of the accreting mass at z=0.25 will by z=0 end up in stars, in the ISM, or be ejected in a wind. In some cases, between $z = 0.25$ and $z = 0$, a particle is ejected multiple times and so at $z = 0$ is again at ISM densities; in those cases we give a preference to the ISM. For $10^{11} M_\odot$ halos, most of the accreting mass ends up in the ISM, while for $10^{11.5} M_\odot$ halos just under half ends up in ISM. For $10^{12} M_\odot$ halos, the distribution is almost completely evenly split amongst stars, ISM, and wind ejection. The contribution of star formation and wind ejection to the mass budget of accreting material is significant. Separately tracking wind ejection and star formation events also gives us a finer time resolution in the gap between $z = 0.25$ and $z = 0$. Note that Table 1 does not imply that galaxies have 50% gas fractions, as most stars formed from gas accreted at $z > 0.25$.
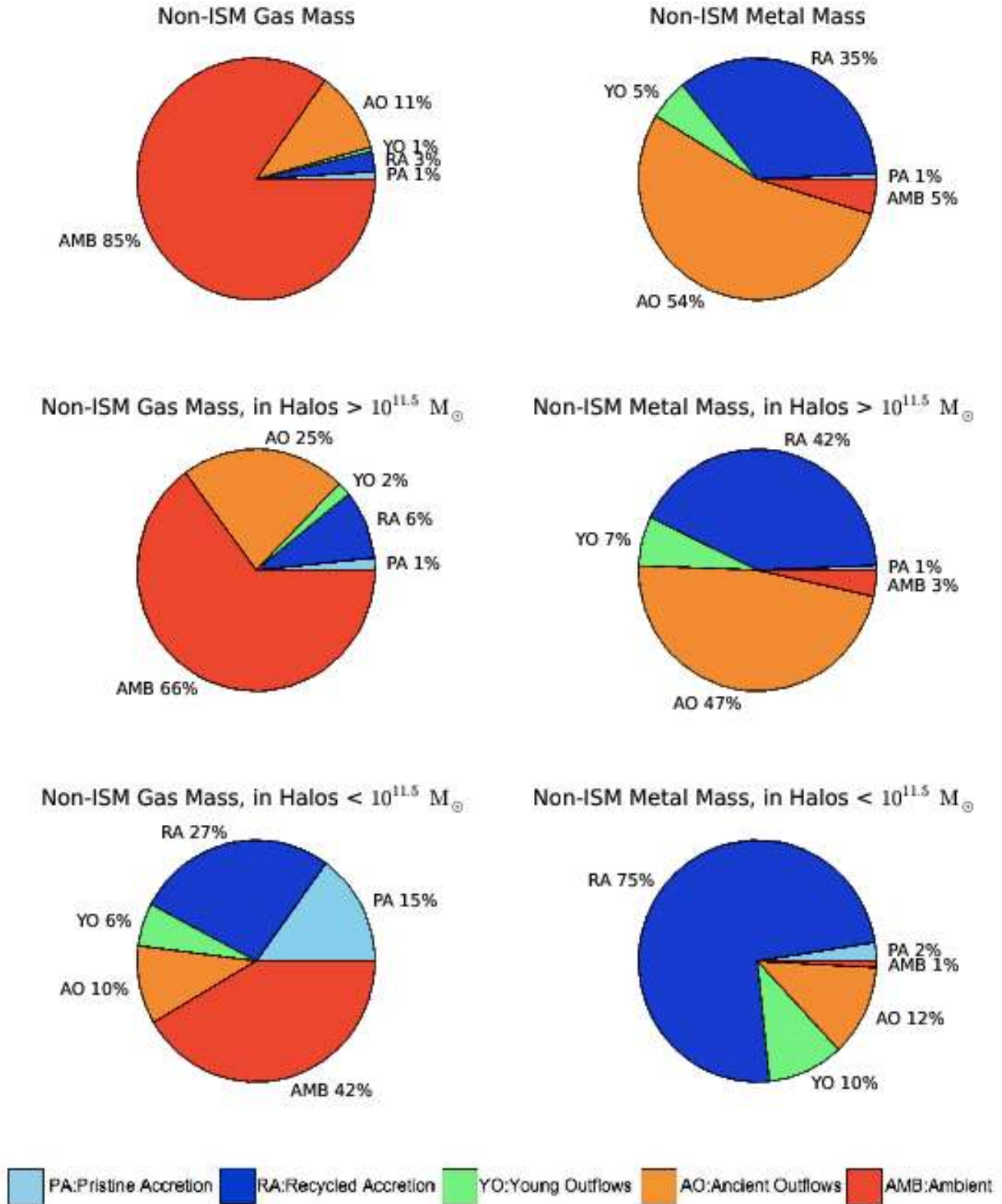
Figure 3. The non-ISM gas mass budget (left) and gas-phase metal budget (right) at $z = 0.25$. Upper plots show the full simulation, and lower plots show only gas within the virial radius of a halo at $z = 0.25$, for high (middle) and low (bottom) mass halos. Ambient is gas that has never been in a wind, before or after $z = 0.25$, that is not accreting. Ancient outflow is for non-accreting gas particles ejected in a wind more than 1 Gyr before $z = 0.25$. Young outflow is for non-accreting gas particles ejected in a wind $\leqslant 1$ Gyr before $z = 0.25$. Recycled accretion is gas that has been ejected in a wind by $z = 0.25$, and will join or pass through the ISM of a galaxy or become a star by $z = 0$. Pristine accretion is gas that has not been ejected in a wind by $z = 0.25$ and will join or pass through the ISM of a galaxy or become a star by $z = 0$.

3.2 Mass Budgets

To begin analysing the gas in these various categories, we first examine their mass fractions. We do this both for all the gas in the simulation and for gas within the virial radius of dark matter halos, which we identify as CGM gas. As we discussed in §1, there are various definitions for CGM in the literature, and in Ford et al. (2013) we argued for 300 kpc as an appropriate radius for the CGM based on the metal absorption extent, at least for $\sim L^*$ galaxies. However, we also showed that the extent of absorption depends on the particular metal ion and there was not a clean distinction between enriched and unenriched regions. Hence, here we will use a CGM definition that is perhaps more removed from direct observations but is well-motivated and well-defined theoretically, namely the virial radius. Our definition for the virial radius is discussed in section § 2. This is at least something that is directly quantifiable and whose extent scales with the galaxy mass.

Figure 3 shows pie charts for the total mass (upper left) and metal mass (upper right) of all non-ISM gas particles in the simulation at $z = 0.25$, broken down by category, while the middle and bottom panels show analogous pie charts considering only non-ISM gas within high- and low-mass halos, respectively. We choose $M_{halo} = 10^{11.5}$ M$_\odot$ as the dividing line between high- and low-mass halos because that is where we see a crossover between hot and cold gas fractions, which we discuss later. We define particles as within the halo if $R \leqslant R_{\rm vir}$. (For reference, we note that ISM gas makes up 1.8% of the total gas mass of the simulation at $z = 0.25$.)

In the upper left panel, we see that most of the non-ISM gas mass in the simulation consists of ambient material. Even though outflows in our simulations are ubiquitous and have mass loading factors typically of unity or above (Oppenheimer & Davé 2008), the majority of baryons in the Universe have never been in a wind since the baryonic fraction in galaxies is small, only 7% in this model. Ambient gas, much of which consists of diffuse gas in the IGM, accounts for 85% of all baryons; this material does not participate in the baryon cycle by $z = 0$ since it has neither been in an outflow nor has it been accreted. Ancient outflow is the next largest category at around 11%, which is still larger than the fraction of baryons in stars (6%), showing that the mass in outflows exceeds that in stars globally, as noted in our earlier simulations (Oppenheimer & Davé 2008). Young ($\leqslant 1$ Gyr old) outflows comprise only about 1% of the mass, which is not surprising since the outflow rate roughly tracks the star formation rate, and this is much smaller at the present epoch than at high redshifts. The global accreting gas mass fraction from $z = 0.25 - 0$ is 4%, of which the vast majority was previously in a wind (3%). Pristine accretion over the 3 Gyr from $z = 0.25$ to $z = 0$ only accounts for 1% of all baryons. Of the material that accretes between $z = 0.25$ and $z = 0$, 25% of it (by mass) is pristine accretion; the other 75% is recycled accretion.

The story is quite different if one considers the metal mass (upper right pie chart). Now ancient outflows contain 54% of all cosmic metals and recycled accretion contains over one-third. Young outflows, which contain only 1% of the total mass, still contain 5% of the metals. Ambient material, having essentially never resided inside a galaxy, contains a

very small amount of metals relative to its mass fraction, and pristine accretion likewise has a negligible metal mass content. The metals that are present in the ambient or pristine accretion gas has three possible sources within our simulations: Type Ia supernova, AGB stars, or tidal stripping. The metals in pristine accreting material mostly owes to tidally stripped ISM material, which then reaccretes. Pristine accretion has an average metallicity of $0.07 Z_\odot$, while recycled accretion has on average approximately solar metallicity. It is worth emphasising that overall accreting material is typically significantly metal enriched, and hence does not usually have low metallicity as is sometimes assumed, at least at these low redshifts.

In the middle and lower panels of Figure 3 we restrict ourselves to only non-ISM material within the virial radius of dark matter halos, i.e. the CGM, which includes roughly 20% of the total gas mass and 70% of the total metal mass of non-ISM gas particles. From the mass fractions in the lower left panels, we see that the fraction of CGM material participating in the baryon cycle is significantly larger for both low- and high-mass halos – the inflow and outflow categories are more prominent. Nonetheless, ancient outflows still dominates over young outflows, and recycled accretion dominates over pristine accretion. High-mass halos have a larger percentage of ambient material, since they can keep their gas hot via a stable virial shock (Birnboim & Dekel 2003) and prevent it from falling back in. The relative contribution of accretion in high-mass halos is smaller than in low-mass ones, also because of temperature: hot halos can prevent infall.

The importance of "halo fountains", i.e. recycled accretion that never leaves the halo, is shown in the metal fraction plot within halos (lower right). For high-mass halos, almost half the metal mass within the halos at $z = 0.25$ will, by $z = 0$, be accreted onto galaxies. The remaining half of the metals are mostly in ancient outflows that are still trapped or recaptured within halos via "outside-in" enrichment (Oppenheimer et al. 2012), with young outflows having a slightly increased metal proportion relative to their gas mass because outflows today are somewhat more metal-rich than outflows at earlier epochs. This owes to the upwards evolution of galaxies along the galaxy mass-metallicity relation in these models (Davé et al. 2011b). For the low-mass halos, the contribution from recycled accretion is dominant: fully 75%. In these low-mass halos, the metals either escape the halo completely or fall back in, whereas in high-mass halos there is a hot halo that can keep the metals bound to the halo but not falling back in.

In Figure 4, we investigate the CGM mass budgets further by breaking down our inflow/outflow categories by their phase. We consider four phases: hot ($T > 10^5$ K), cold ($T < 10^5$ K), ISM ($n_H \geqslant 0.13$ cm^{-3}), and stars. The top panel shows the fractional CGM gas mass, relative to the total mass, by phase as a function of halo mass. The black line shows the total baryonic fraction, which hovers around but is slightly below the universal baryon fraction of 0.164, (dot-dot-dot-dash horizontal line), until it starts to drop at $M_{\rm halo} \lesssim 10^{11.5} M_\odot$. The hot and cool gas fractions cross over at roughly this mass, with the CGM becoming hot gas-dominated at higher masses as is typically seen in these types of simulations (e.g. Kereš et al. 2005; Gabor & Davé 2012; Nelson et al. 2013). (This crossover
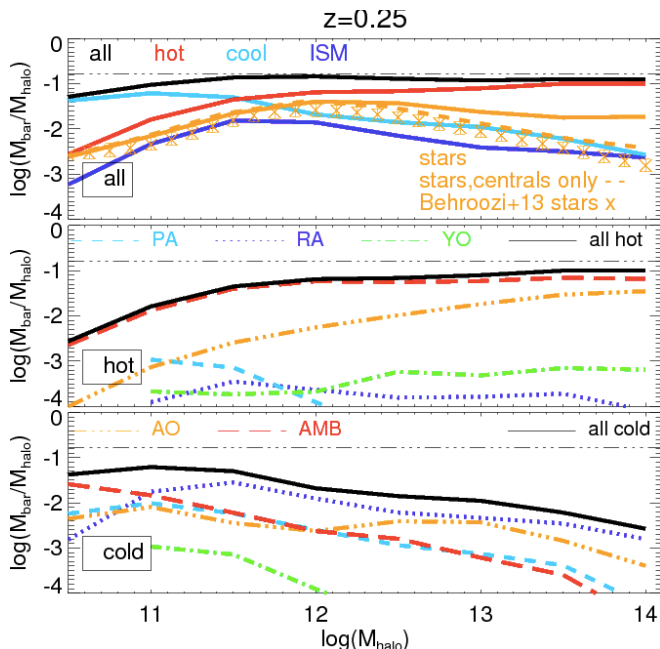
Figure 4. Upper panel: the fraction of baryons that are hot ($>$ 10^5 K; red) , cool ($< 10^5$ K; light blue), the ISM (i.e. star-forming; dark blue), and in stars (orange) vs. halo mass at $z = 0.25$. We plot the total baryon fraction in halos (solid black). The black horizontal dot-dot-dot-dash line represents the global ratio Ω_b/Ω_m. We also plot the fraction of baryons in just the hot phase (middle panel) and the cold phase (bottom panel) vs. halo mass divided into categories as labelled.

.

also serves as justification for the mass breakouts shown in Figure 3.) The stellar and ISM gas fractions have a peak at $M_{\rm halo} \approx 10^{12} M_\odot$; star formation is suppressed at lower masses by increasingly strong outflows and at higher masses by our quenching prescription. The overall shape agrees reasonably well with that inferred from halo abundance matching studies at $z = 0.1$ (e.g. Behroozi et al. 2013). As shown in Behroozi et al. (2013), there is very little evolution in $M_{\rm bar}/M_{\rm halo}$ as a function of $M_{\rm halo}$ from $z = 1$ to $z = 0.1$, so comparing this work's $z = 0.25$ data to Behroozi et al. (2013) at $z = 0.1$ is acceptable. There are some differences at higher masses, because we include satellites in the stellar content of our halos while Behroozi et al. (2013) does not include them. As shown in Berlind et al. (2003), satellites make a larger contribution to the stellar mass budget at larger halo masses. If we exclude satellites (orange dashed line), we get much better agreement with Behroozi et al. (2013). This is essentially equivalent to saying that the stellar mass function in this model agrees well with the observations, which was shown directly by Davé et al. (2013).

In the middle and lower panels we consider the hot and cold (non-ISM) CGM components, demarcated at $10^5 K$, and split them in our inflow/outflow categories as labelled. The black lines show the total hot (red line in upper panel) and total cool (light blue in upper panel) fractions for reference. The hot phase is completely dominated by ambient gas at all masses. This indicates that hot halo baryons are generally not participating in the baryon cycle, at least in our simulations. Ancient outflows are approximately an order of

magnitude smaller in mass fraction, except at the largest masses where the outflows are more efficiently retained or re-accreted within group potentials and rise to become half the ambient gas mass. The other categories provide an essentially negligible contribution to the hot gas. We note that in our models we eject the winds at the ISM temperature, which are then allowed to interact with the CGM gas once it escapes the ISM. However, given that it is metal enriched it tends to cool quickly even if it shock-heats initially. This enhances the recycling of that material, and hence hot halo gas contains little of this component.

By contrast, the cool phase has more mass undergoing baryon cycling. For halos with $M_{\rm halo} > 10^{11} M_\odot$, recycled accretion dominates the mass budget, owing to short recycling times in massive halos (Oppenheimer et al. 2010). For smaller mass halos, ambient gas again dominates, and pristine accretion becomes the most important accretion channel. This transition from enriched to pristine accretion in the cool gas could provide an interesting signature of recycling in absorption lines.

To recap, we divide all non-ISM gas at $z = 0.25$ into five categories: **pristine accretion**, which holds a small fraction of both the total gas mass and the metal mass but dominates accretion in dwarf galaxy halos; **recycled accretion**, which dominates accretion for sizeable halos and holds a substantial fraction of their metal mass; **young outflows**, which are a sub-dominant component of mass and metals in the CGM, **ancient outflows**, which hold roughly half the total metal mass in the CGM; and **ambient material**, which contains a small fraction of the metals but a majority of the gas mass, particularly the hot gas mass, both globally and within the CGM.

3.3 Relation to Dynamics

We have defined inflows and outflows based on their future and past history relative to $z = 0.25$. It is interesting to see how these definitions relate to the actual dynamics of the gas at $z = 0.25$. One expected trend would be that outflows, particularly young outflows, should have an outward radial velocity relative to the galaxy and that inflowing gas should have a negative radial velocity. To examine this, we calculate the radial velocity v_r of gas particles relative to the nearest central galaxy, and compare it to the halo virial velocity $v_{\rm vir}$.

Figure 5 shows $v_r/v_{\rm vir}$ vs. wind age for all non-ISM particles in the simulation. For ages in the range of roughly 10^7 to 10^9 years, our dividing line between young and ancient outflows, there is a clear asymmetry in this distribution towards positive v_r, i.e. outflowing gas, which is much more pronounced for more recently ejected winds. A more subtle trend is that, excluding the gas that is in the outflowing "plume" to small age and large v_r, there is a negative velocity for the remaining wind gas. This corresponds to wind recycling, which we will explore in more detail below. Despite the presence of clearly outflowing gas, even recent outflows can span a range of velocities, including negative. This indicates that instantaneous radial velocity alone is not a robust identifier of relatively recent ejection.

Another approach to examining how our adopted categories relate to the dynamics of the gas is to look at velocity-radius plots. In such plots, the outflows would be expected to have a large positive radial velocity close to galaxies, di-
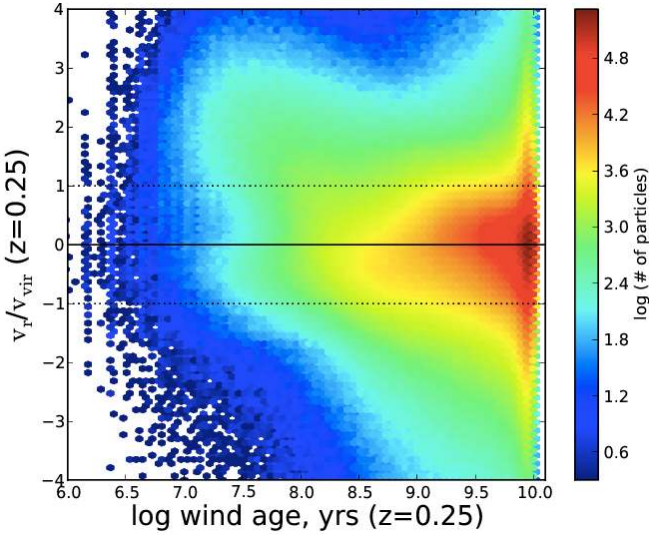
Figure 5. v/v_{vir} vs. wind age for all non-ISM gas particles in the simulation at $z = 0.25$

minishing as it moved further away, while inflows might be expected to show up as a net negative velocity, perhaps increasing as one approaches a galaxy.

Figure 6 shows the radial velocity (scaled to the virial velocity) versus radius (scaled to the virial radius) split into our categories as labelled. We associate each gas particle with the galaxy to which it is most bound. Because satellite galaxies can both eject winds and accrete gas, which could confuse our analysis, in these plots we restrict ourselves to gas particles associated with central galaxies. The scale for each panel is logarithmic in particle number, and spans the same range in each panel for ease of comparison. We note that each category does *not* have the same number of particles. The top two panels show accretion, pristine (left) and recycled (right). The middle two panels show young (left) and ancient (right) outflows. The bottom panels show ambient gas (left) and the sum of all the categories, i.e. all non-ISM gas (right). The solid line indicates zero velocity and the dotted lines delineate the virial velocity.

We begin by looking at all gas particles in the simulation, not in the ISM at $z = 0.25$ and associated with central galaxies (lower right panel). With the exception of an inflowing plume at large r/r_{vir}, which we discuss in more detail below, in general the distribution is fairly symmetric. The distribution is also fairly smooth: there is not a neat "outflow" plume, a tight "inflow" plume, or a distinct "rotating with disk" component. Rather, one sees a more ambiguous picture, and hence robustly deciding which positive velocity gas to call outflows versus rotation or ambient motion can be quite difficult. This is why we choose to make our distinctions not based on the velocity, but in the manner described in §2.1

Looking at the different categories, pristine accretion (upper left) has the peak of its distribution at or slightly less than zero, depending on r/r_{vir}, indicating an inflow. There is also a slight inflowing plume at large radius, as seen in the "all non-ISM" panel. It is remarkable that so much pristinely accreting material has positive velocities, and it shows that accretion is not so easily identified as merely inward-moving

gas. There is a lot of random motion in the halo, so even material that will eventually accrete (onto either a central or satellite galaxy) can be moving away from the central galaxy, as shown here. Recycled accretion (upper right) shows similar trends: the peak of its distribution (yellow region) is shifted slightly below zero, but much of the material has a positive velocity, especially at radii $\approx 0.1 r_{\mathrm{vir}}$. This is recent wind material, which will turn around and accrete by $z = 0$.

The middle two panels show the outflows, young (left) and ancient (right). The young outflows show a distinct asymmetry towards outflowing gas. However, at any radius, young outflows are both moving towards and away from the galaxy. In other words, there is not an obvious demarcation in radial velocity that will uniquely isolate outflows occurring within the last $\approx$ Gyr. One could demarcate the plume at high v_r and low r, but this will contain only a small fraction of the young outflowing material. Meanwhile, the ancient outflows show, unsurprisingly, even less asymmetry, with the exception of the the same inward plume seen earlier.

The ambient gas (lower left) shows essentially perfect symmetry about $v = 0$, as one would expect for gas that is neither in a wind nor going to be accreted. However, there is a strong concentration within the large radius plume, which is seen in the other panels as well. This owes to massive halos only ($> 10^{11.5}$ $M_\odot$); lower mass halos do not have this feature. This plume simply owes to the gravitational growth of structure, as gas falls into halos at large radii. Such gas gives rise to an infall signature at large radii as observed at $z \sim 2$ (Rudie et al. 2013). However, once it falls into the halo, ambient gas does not continue its motion towards the galaxy, but instead settles into a virialised halo that has essentially no net velocity relative to the galaxy.

In summary, the various categories of inflow and outflows show distinct trends in their kinematics. Accretion has a net negative inflow, although some of that material has positive velocities. Young outflows have a distinct asymmetry towards having more outwards moving gas, but there is still a wide range of radial velocities in this category, even at small radii. In terms of wind age, the youngest outflows show a clear outflowing tendency, but this signature mostly disappears for wind ages above a Gyr. Such ancient winds show little net infall or outflow from within the halo, and in many ways are much more like ambient material. Generally, it is difficult to separate these categories cleanly using cuts in velocity space, even when one includes radial distance information.

4 OBSERVABLES

With a better understanding of the dynamical state of the CGM in hand, we now turn our focus to the observable signatures of accretion, outflows, and ambient material. In principle, a sufficient suite of observed absorption line tracers could directly constrain both the physical state and dynamics of the gas relative to a nearby galaxy. However, in practice, absorbers around halos are sparse and are not commonly visible in multiple metal tracers. Together with the uncertainty over the multi-phase nature of CGM, it is challenging to extract robust information directly from the data. Hence simulations such as ours can provide some insights
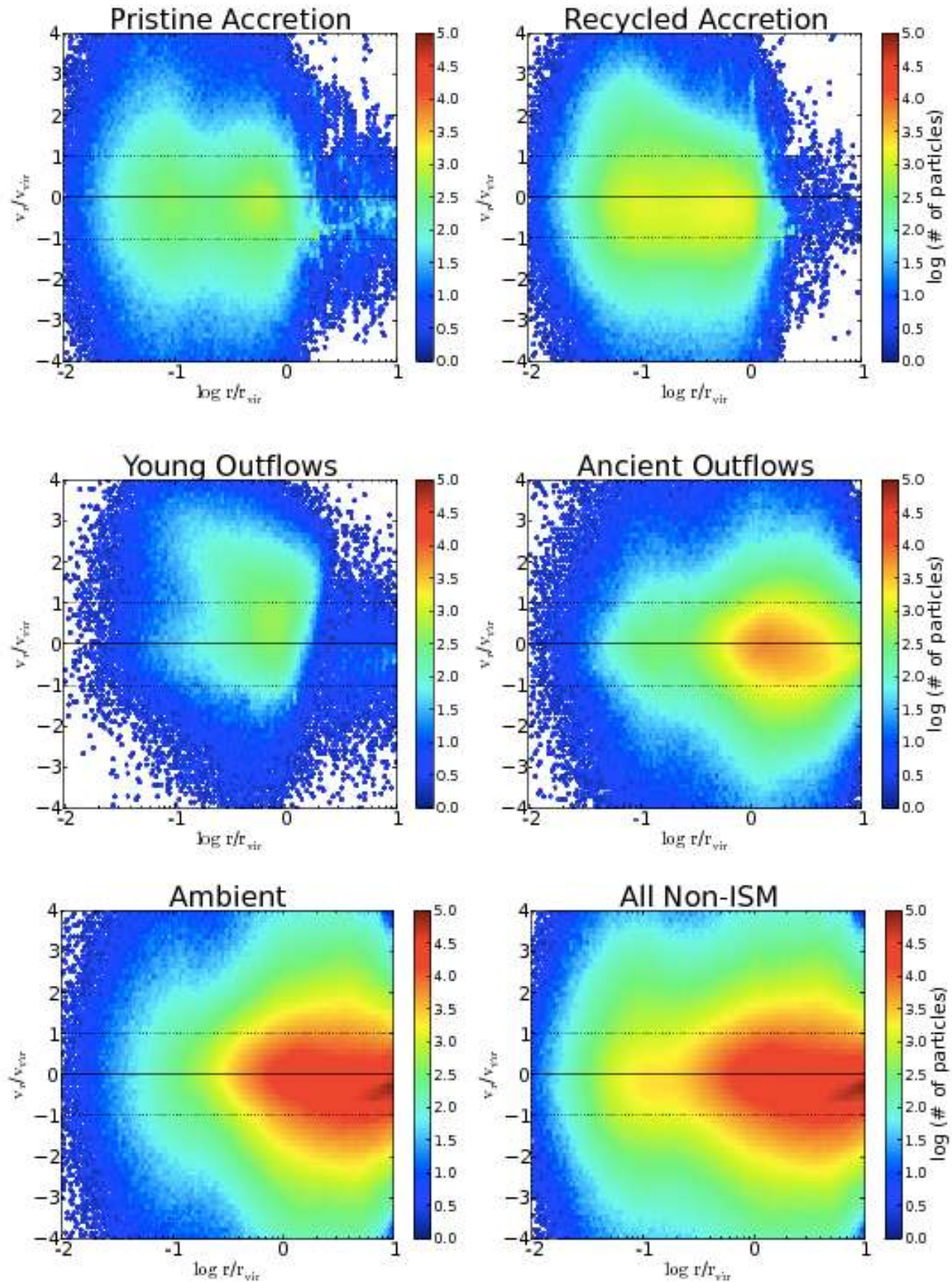
Figure 6. V · r/abs(r) (divided by the virial velocity) vs. radialdistance from the host galaxy (divided by the virial radius), for non-ISM gas at $z = 0.25$ divided into each of the categories as labelled. To guide the eye, we have added solid horizontal lines at v = 0, and dotted horizontal lines at v = $\pm$v$_{\rm vir}$.

into mapping specific ions onto gas with specific physical and dynamical properties.

In Ford et al. (2013) we focused on how absorbers trace the physical conditions of the gas, namely the density and temperature. Here, we extend this to now consider the dynamical state of the gas, and determine whether there is some reliable mapping between certain absorption line tracers and whether gas is inflowing, outflowing, or ambient.

4.1 Column Density vs. Impact Parameter

In Figure 7 we plot the mean column density per line of sight of different species (as labelled) versus impact parameter for galaxies with a halo mass of $10^{11} M_\odot$ (left panels) and $10^{12} M_\odot$ (right panels). We start at 10 kpc, which is the typical extent of the ISM, and go out to 300 kpc, roughly delineating the CGM as argued in Ford et al. (2013). We compute this by summing the column density within ± 300 km s^{-1} of the galaxy (for all lines of sight), and then divide by the number of lines of sight. We choose to plot a mean versus a median to promote a fairer comparison with the data, since a median is sensitive to the (often variable) detection threshold. We then subdivide the mean column density by inflow/outflow category. In practice, we create a simulation snapshot containing only gas particles of a given category, obtain absorption spectra using `Specexbin` (Oppenheimer & Davé 2008), and get column densities by fitting Voigt profiles using `AutoVP` (Davé et al. 1997). The solid black line is for all the gas in the simulation, and the coloured broken lines show the breakdown by category, as indicated in the legend. The solid black line is akin to what an observer would actually see, the coloured lines are what an observer would see if the universe consisted only of gas in the labelled category.

Looking at HI absorption in L^* halos ($10^{12} M_\odot$; top right panel), we see that recycled accretion provides the dominant contribution at impact parameters less than about 75 kpc (all distances are physical). Beyond that, ambient gas and ancient outflows make up the bulk of the absorption. In $10^{11} M_\odot$ halos (top left panel), ambient gas dominates at all impact parameters greater than about 25 kpc, followed by ancient outflows. At very small radii, recycled accretion also becomes important for low-mass halos. Both theoretical and observational works have claimed that accretion can be probed via high-column density HI lines (Fumagalli et al. 2011; van de Voort et al. 2012; Lehner et al. 2012) and our results support this claim, although in our case we are probing lower column density gas than the Lyman Limit systems (LLS) typically considered in those works. In our case, the typical column density at 25 kpc is 10^{15}cm^{-2}, which is well below a LLS but strong nonetheless.

For Mg II, the majority of absorption owes to recycled accretion at all impact parameters and at both halo masses. Outflowing material altogether provides a much lower contribution to the absorption; close in, young outflows are more prominent, while beyond 50 kpc ancient outflows contribute more. Low-metallicity gas, i.e. pristine accretion and ambient gas, makes only a negligible contribution. At all impact parameters, Mg II traces gas that will fall into galaxies by $z = 0$. Physically, gas in our simulations that is sufficiently cold and dense to give rise to Mg II absorption cannot support itself against gravity, and hence accretes on a dynamical

timescale. Thus our simulation indicates a tight connection between Mg II absorption and star formation that occurs within 1-2 dynamical timescales.

The story is similar for Si IV: recycled accretion is the most important source for absorption at all impact parameters and halo masses. However, it is less dominant than in the Mg II case. Once again young outflows dominate the outflow contribution close in, but the crossover point with ancient outflows occurs farther out, at ≈ 50 kpc. Hence Si IV, despite its rather high ionisation state, behaves much like Mg II because the typical temperature and density giving rise to Si IV absorption is more similar to Mg II than to that of higher ions (Ford et al. 2013).

For C IV the behaviour changes somewhat and also becomes more dependent on halo mass. For $10^{12} M_\odot$ halos at low impact parameters, recycled accretion provides the dominant contribution to the total absorption, but beyond about 100 kpc ancient outflows become the largest contributor. For $10^{11} M_\odot$ halos, within 50 kpc, recycled accretion, young outflows, and ancient outflows all are equally important, while at larger impact parameters ancient outflows dominate, followed by recycled accretion and then young outflows. Hence, depending on the impact parameter and the halo mass, C IV can trace recycled winds, and either young or ancient outflows.

For the high ions O VI and Ne VIII, recycled accretion dominates at small impact parameters in large halos, otherwise ancient outflows dominate. Interestingly, the shape of the black line for the high ions is flatter than for low or mid level ions – the strength of the absorption depends less on the proximity to the galaxy, as noted by Ford et al. (2013).

Material that has never been in a wind (ambient or pristine accretion) does not provide a significant amount of absorption in metal lines. For H I, however, ambient gas plays a major role, more than any other category at radii $\geqslant 75$ kpc. This is not surprising given the huge amount of mass contained within the ambient gas, as seen in Figure 3. However, at radii $\leqslant 75$kpc, recycled accretion provides the dominant contribution for H I and this region typically contains the strongest H I lines (Ford et al. 2013). Hence, recycled accretion likely dominates the high-column density H I absorbers at $z = 0.25$.

In summary, we see distinct trends in the type of material traced by absorption as a function of ionisation potential. Low metal ions, particularly close to galaxies, generally arise from recycled accretion, while high ion absorption is from ancient outflows. This latter finding is consistent with the analysis of Tumlinson et al. (2011), who detect large amounts of O VI in the CGM and determine that it must have been generated by protracted earlier epochs of star formation and winds.

4.2 Fractional Column Density Distributions

Column density distributions (CDDs) provide a more detailed look at the strengths of individual absorbers within our various categories. Figure 8 shows the "fractional CDD" for each of our ions, for our two halo mass bins ($10^{11} M_\odot$ left panels, $10^{12} M_\odot$ right panels), at an impact parameter of 25 kpc (upper panels) and 100 kpc (lower panels). The lines are colour-coded by category: pristine accretion (light blue), recycled accretion (dark blue), young outflows (green), an-
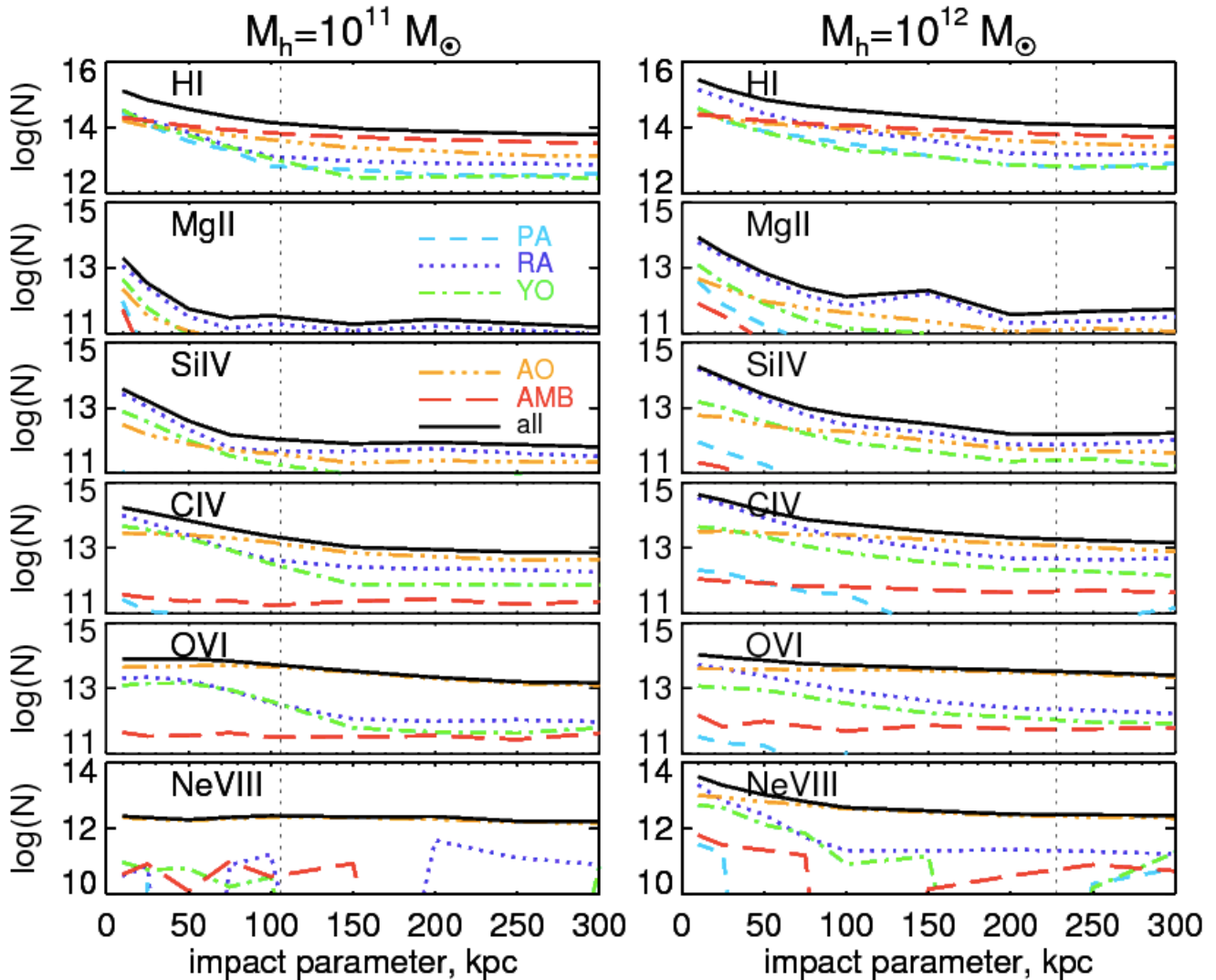
Figure 7. The average column density per LOS for targeted lines of sight around $10^{11} M_\odot$ (left panels) and $10^{12} M_\odot$ (right panels) halos for different species (as labelled). The black solid line includes all the gas. Coloured lines indicate results from including only absorption from: pristine accretion (light blue dashed), recycled accretion (dark blue dotted), young outflows (green dot-dashed), ancient outflows (orange dot-dot-dashed), and ambient (red long-dashed). Vertical lines indicate the approximate virial radius at the midpoint of each mass bin. Note the yrange is not the same for each ion, though it always spans 4 dex.

cient outflows (orange), and ambient gas (red). We define fractional CDD as the fraction of the total absorption *in that column density bin* that owes to a given category. Where colored lines do not extend, there are no absorbers in that particular column density bin. In some cases the lines do not add up to one, that is because occasionally there is contribution from ISM gas (not plotted here) to the total. For Ne VIII at 100 kpc, we note that the colored lines overlap in some cases.

In these plots we can identify some general trends as a function of ionisation potential. For HI, there is more strong absorption from recycled accretion than pristine accretion. At impact parameters of 25 kpc in $10^{12} M_\odot$ halos the strongest metal lines are almost always dominated by recycled accretion. The trend is particularly strong for low ions and is even true for O VI, although strong Ne VIII lines have comparable contributions from both young and old outflows. Strong metal absorption at this impact parameter traces ma-

terial that will fall into the galaxy within a few Gyr; just as for the strongest H I absorbers. At lower metal columns outflows become important and can even dominate. Generally young outflows are more important for lower ions and ancient outflows are more important for higher ions. Low column HI absorption owes mostly to ambient gas and less to ancient outflows. These trends also hold for $10^{11} M_\odot$ halos except that ancient outflows now dominate at all columns for the high ions.

At an impact parameter of 100 kpc for $10^{12} M_\odot$ halos, the trends look somewhat different. For low ions the strongest observable metal lines still come from recycled accretion, but the contribution from outflows can be significant at lower columns, and at this larger impact parameter it is almost always ancient outflows that are more important than young outflows. It is likely that the low ions still arise from gas close to galaxies, but perhaps close to substructures such as what is seen in Figure 1. In contrast, O VI is
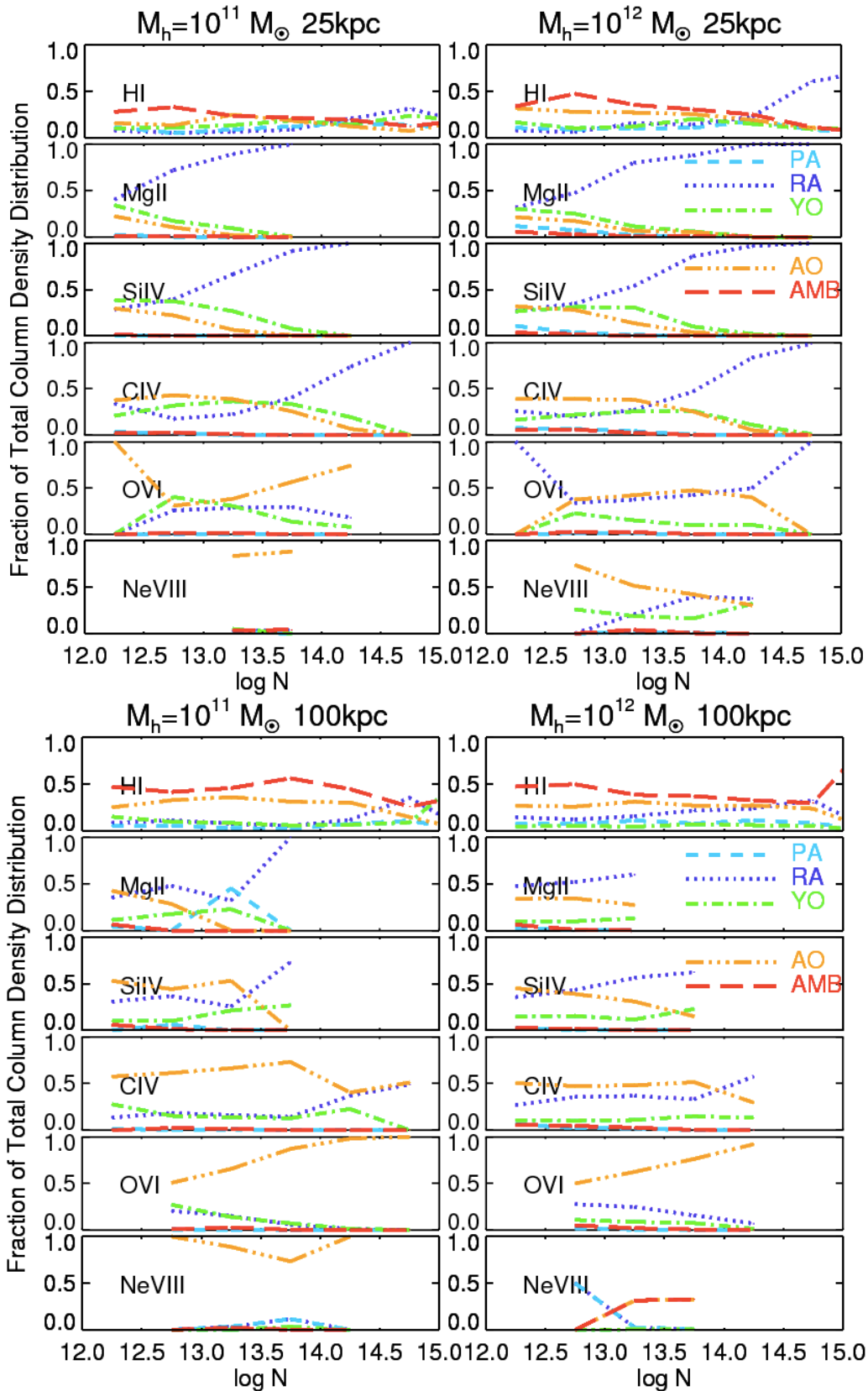
Figure 8. Fractional column density distributions, i.e. the fraction of absorption in bins of size $\log N = 0.5$ owing to the various categories for different species (as labelled) at impact parameters of 25 kpc (top panels) and 100 kpc (bottom panels), for $10^{11} M_\odot$ halos (left panels) and $10^{12} M_\odot$ halos (right panels). Where lines do not extend, there is no column density in that bin from any gas.

completely dominated by ancient outflows, consistent with the findings of Oppenheimer & Davé (2009). Young outflows contribute but do not dominate at any column density. For our mid ion C IV, the main contribution is from ancient outflows except for very strong absorbers around $10^{12}M_{\odot}$ halos, where recycled accretion is prominent. Meanwhile, the H I is usually dominated by ambient gas with important contributions from ancient outflows for both halo masses with recycled accretion also becoming important at higher columns.

4.3 Covering Fractions

A key observable is the covering fraction of absorbers down to some particular column density or equivalent width limit. Here we sum all absorbers within $\pm$ 300 km/sec of the targeted galaxy for each of our lines of sight, above an equivalent width limit of 0.05Å. We use summed equivalent widths rather than individual components to minimize sensitivity to details of the line identification and deblending algorithm.

Figure 9 shows the covering fractions for our various ions, for our two halo mass bins. The total is shown as the black line and can be compared to what is observed. The coloured lines show the theoretical covering fraction including only the gas in the labelled category. Note that the coloured lines do not sum to the black line – we compute the covering fraction of each category individually above our chosen equivalent width limit of 0.05Å.

HI has a near-unity covering fraction at all impact parameters and halo masses, owing mostly to ambient gas. Ancient outflows have large covering fractions within $\sim$ 100kpc for both halo masses and recycled accretion also becomes substantial for $10^{12}M_{\odot}$ halos. Pristine accretion and young outflows also have comparable non-trivial covering fractions for both halo masses but it is clearly much smaller than recycled accretion in $10^{12}M_{\odot}$ halos. Hence even HI does not typically trace pristine inflows in these halos, because as we showed in Fig 3, the accreting mass budget is actually dominated by recycled accretion at these epochs.

As expected, the metal lines almost never show significant covering fractions from either ambient or pristine accretion, as the metal content tends to be quite low. The remaining categories follow trends similar to those seen for the column densities: low ionisation line covering fractions tend to be almost always dominated by recycled accretion, while C IV is dominated by recycled accretion close in but by ancient outflows further out. O VI is dominated by ancient outflows everywhere, except for at very low impact parameters around $10^{12}M_{\odot}$ halos . Qualitatively, this trend holds for all halo masses, although the overall metal line covering fraction, particularly at small impact parameters, falls towards smaller halos.

These results are intended to qualitatively illustrate the behaviour of covering fractions, and show that they mimic trends seen in other statistics. We will present a more detailed comparison of covering fractions versus COS-Halos data, including covering fractions as a function of equivalent width, using simulated spectra chosen to match the COS-Halos sample, in an upcoming paper (Ford et al. 2014, in preparation).

5 PHYSICAL CONDITIONS

5.1 Mass and metal profiles

To better understand why the absorption patterns detailed in the previous section arise, we now examine the physical conditions in the halo associated with the inflowing and outflowing gas. We begin by considering the mass and metal profiles associated with our various categories. Figure 10 shows these profiles as a function of $R/R_{\rm vir}$, out to the virial radius. We emphasize this is a 3-D radial profile, not projected as impact parameter. The left panels show the mass fraction as a function of radius in each category, while the right panels show the metal fractions. The two rows show our two halo mass bins. We include only gas around central galaxies, since our LOS are only around central galaxies. As explained in §3.3, each gas particle is assigned to a galaxy to which it is most bound. If a particle is assigned to a satellite galaxy we do not include it in Figure 10.

Let us first consider recycled accretion. Broadly speaking, for both mass bins, the percent of gas mass and metal mass in recycled accretion decreases with increasing $R/R_{\rm vir}$. This soon-to-be recycled material is fairly close to galaxies, which explains why it is predominantly found in cooler, denser gas and explains why HI at low impact parameters comes more from recycled accretion than from ambient gas. In Figure 7 we noted that, at least for the more massive halos, metal absorption from recycled accretion is fairly strong close to galaxies, while ancient outflows become more dominant at larger impact parameters. This is why in the case of the $10^{12}M_{\odot}$ halo at low impact parameters there is substantial absorption in O VI from recycled wind material – because very close to $10^{12}M_{\odot}$ galaxies, most of the metals are found in recycled accretion material. Hence, even though much of the recycled wind material close to galaxies is cool and dense, the high enrichment level still allows for significant O VI absorption. Meanwhile, the low metal ions have rapidly dropping absorption profiles with radius, while high ions have radial profiles that are more flat. The low metal ions necessarily arise in cool, enriched gas, which typically has a short recycling time. In $10^{12}M_{\odot}$ halos the recycled accretion is peaked within r<0.3$R_{\rm vir}$, while for $10^{11}M_{\odot}$ it is spread more smoothly out to $R_{\rm vir}$.

For pristine accretion, we see that the percentage of the gas and metal mass also drops with increasing $R/R_{\rm vir}$. The percentage of mass in ambient gas increases with radius, becoming the dominant component at large radii, but the ambient gas contains few metals. The percentage of the gas mass in ancient outflows changes little with radius, but the percentage of the metal mass increases appreciably. The percentage of mass in young outflows is fairly flat with radius but the metal mass rises. These profiles set the baseline for where metals are located within the CGM, which is then convolved with the physical conditions to give rise to the actual amount of absorption.

5.2 Velocity and kinematics

We can also track the kinematics of our absorbers, as shown in Figure 11. In this Figure we focus on Mg II and O VI, as examples of low and high ions. We include only recycled accretion (blue), young outflows (green), and ancient outflows
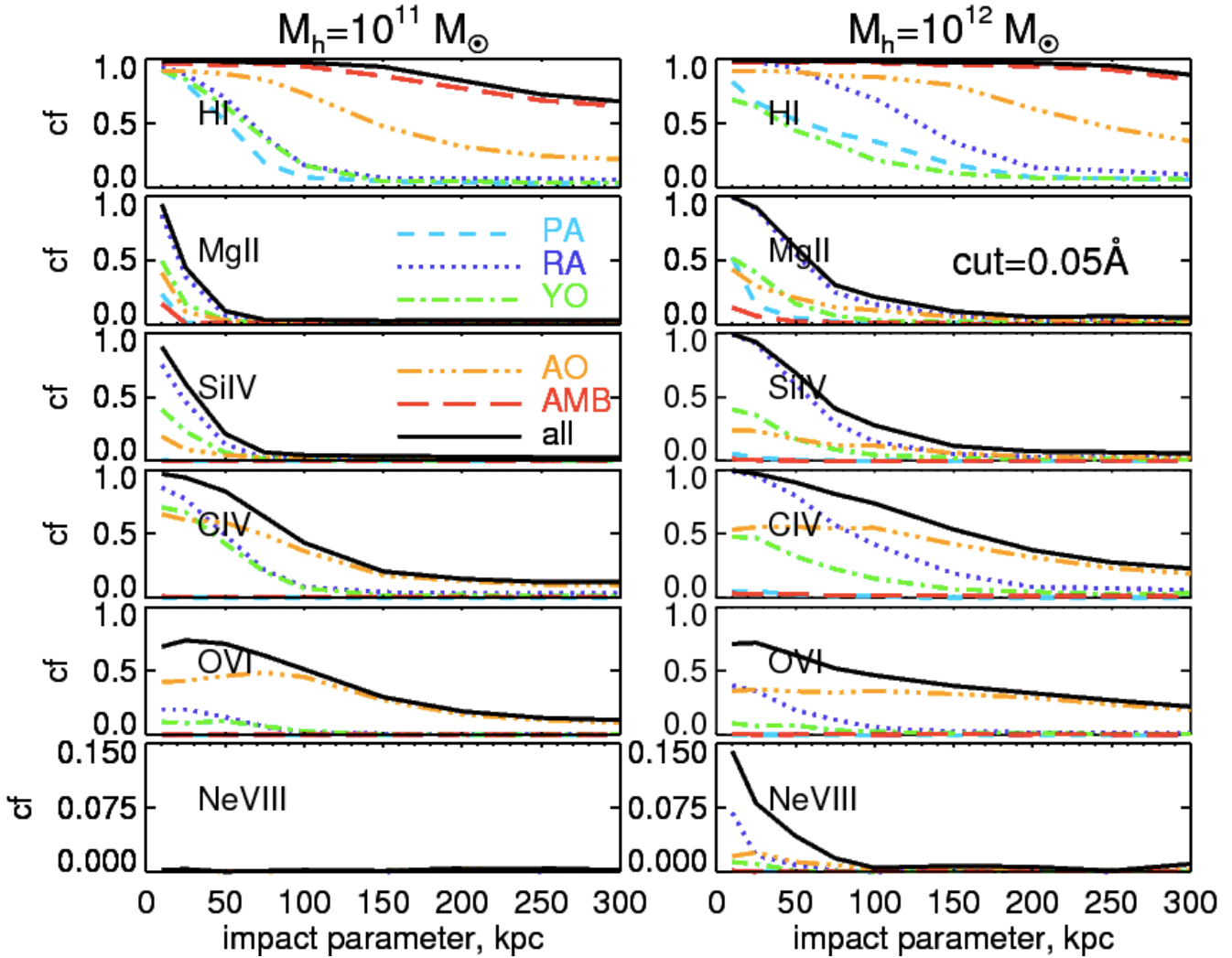
Figure 9. Covering fractions for $10^{11} M_\odot$ (left panels) and $10^{12} M_\odot$ (right panels) halos, showing the fraction of sight lines with equivalent widths > 0.05Å for the species as labelled. The black line includes all the gas and the broken coloured lines are split into the categories as labelled. Note the different y-axis range for Ne VIII, and note that individual categories are computed separately and do not sum to the black line.

(orange), since the other categories do not contribute significantly to the metal absorption. To measure the kinematics of CGM absorbers relative to their galaxy, we subtract the galaxy's systemic velocity and plot a histogram of the velocities of the absorbers. Here we show components, not systems, and all absorbers above 30 mÅ are plotted. We show both halo bins, $10^{11} M_\odot$ and $10^{12} M_\odot$, at impact parameters of 25 kpc and 100 kpc. For comparison we show the approximate escape velocity ($v_{esc} = \sqrt{2GM/r}$) as dashed lines, using the impact parameter (25 kpc or 100 kpc) as the radius and the midpoint of each mass bin as the mass.

For both the $10^{12} M_\odot$ and $10^{11} M_\odot$ halos we see that most of our absorbers lie within the escape velocities of their host halos, at least at these impact parameters, for both Mg II and O VI. We note that for $10^{12} M_\odot$ halos, this is true by definition, as we only consider those absorbers within ± 300 km s^{-1} as associated with a galaxy, and the escape velocity at these impact parameters is $\geqslant 300$ km s^{-1}. However, one can see the distribution trailing off; even if we did not make this cut at 300 km s^{-1} it is unlikely we would see

significant numbers of absorbers past 300 km s^{-1}. In general, the shape of the velocity distributions for the different categories are similar, showing that there is no strong kinematic trend that distinguishes inflow from young or ancient outflow.

5.3 Phase Space Plots

A key diagnostic of the physical conditions of an absorber is its location in the temperature-overdensity phase space. In Ford et al. (2013) we extensively examined the location of absorbers in this phase space using similar simulations. Unsurprisingly, we found that low ionisation potential absorption like Mg II arises in cooler, denser environments, while high ionisation potential absorption such as O VI and Ne VIII exist in warmer, more diffuse environments, with Si IV and C IV being intermediate (see Figure 6 of Ford et al. 2013). Here we expand on that work by examining where our different inflow/outflow categories lie in phase space, and which absorbers might be tracing such gas. We focus here on Mg II,
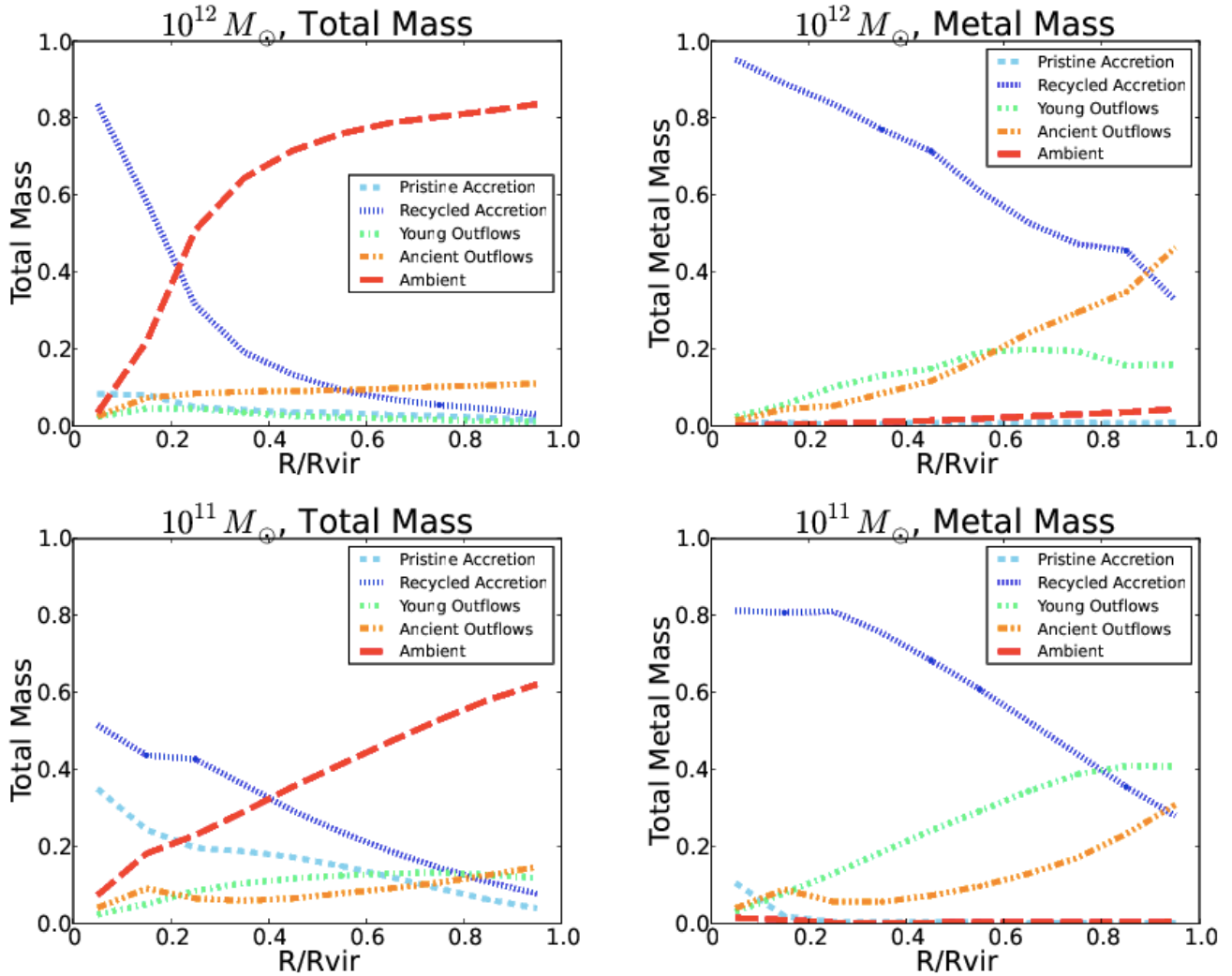
Figure 10. Left panels: fraction of the total mass of non-ISM gas particles in various categories as a function of R/R_{vir} at $z = 0.25$, as labelled. Right panels: fraction of the total *metal* mass. Top panels are for $10^{12} M_\odot$ halos and the lower panels are for $10^{11} M_\odot$ halos. Only central galaxies are considered.

C IV, and O VI as representative of low, mid, and high ionisation potential lines; other transitions follow trends based on their ionisation potential. We will also examine HI in pristine accretion and ambient gas, since this gas generally gives rise to weak if any metal absorption.

In Figure 12, we show phase space contours of halo gas in each category at $z = 0.25$ (first 5 panels), as well as all non-ISM gas particles (last panel) within halos. The legend for the coloured contours is indicated on the right, showing the logarithmic number density of particles at each position in phase space; for ease of comparison it is the same in all panels, even though not all the categories have the same total number of particles.

In the recycled accretion, young outflow, and ancient outflow panels we overplot, as the black symbols, the location in density and temperature space of Mg II (x's), and O VI (filled circles) absorbers that arise from particles in that category. For clarity, we have only plotted the strong absorbers ($N > 10^{14}$ cm^{-2}), and only around $10^{12} M_\odot$ halos at impact parameters of 25 kpc. In the pristine accretion and ambient

panels, there are no strong Mg II or O VI absorbers around $10^{12} M_\odot$ halos at 25 kpc. Instead, we plot the H I absorbers around $10^{12} M_\odot$ halos at 25 kpc, for the strengths as labelled.

Both pristine (upper left) and recycled (upper right) accretion consist almost exclusively of cooler ($T < 10^5$ K) gas. Gas at temperatures $T > 10^5$ K is unlikely to accrete onto galaxies between $z = 0.25$ and $z = 0$. Nonetheless, there is some recycled accretion gas extending up to hotter temperatures at moderate overdensities ($\sim 10^3$), where the cooling time becomes sufficiently short that gas can radiate away its thermal energy.

Considering metal lines, Mg II absorbers trace the densest recycled accretion gas, typically with $\delta > 10^4$, while O VI traces more diffuse and often significantly hotter halo gas. Both O VI and Mg II arise from recycled accretion at 25 kpc, but never from the same phases of this gas! Much of the absorption arises in cooler photo-ionised gas, but the hotter plume of recycled accretion gas mentioned above gives rise to substantial O VI absorption as it transitions through the
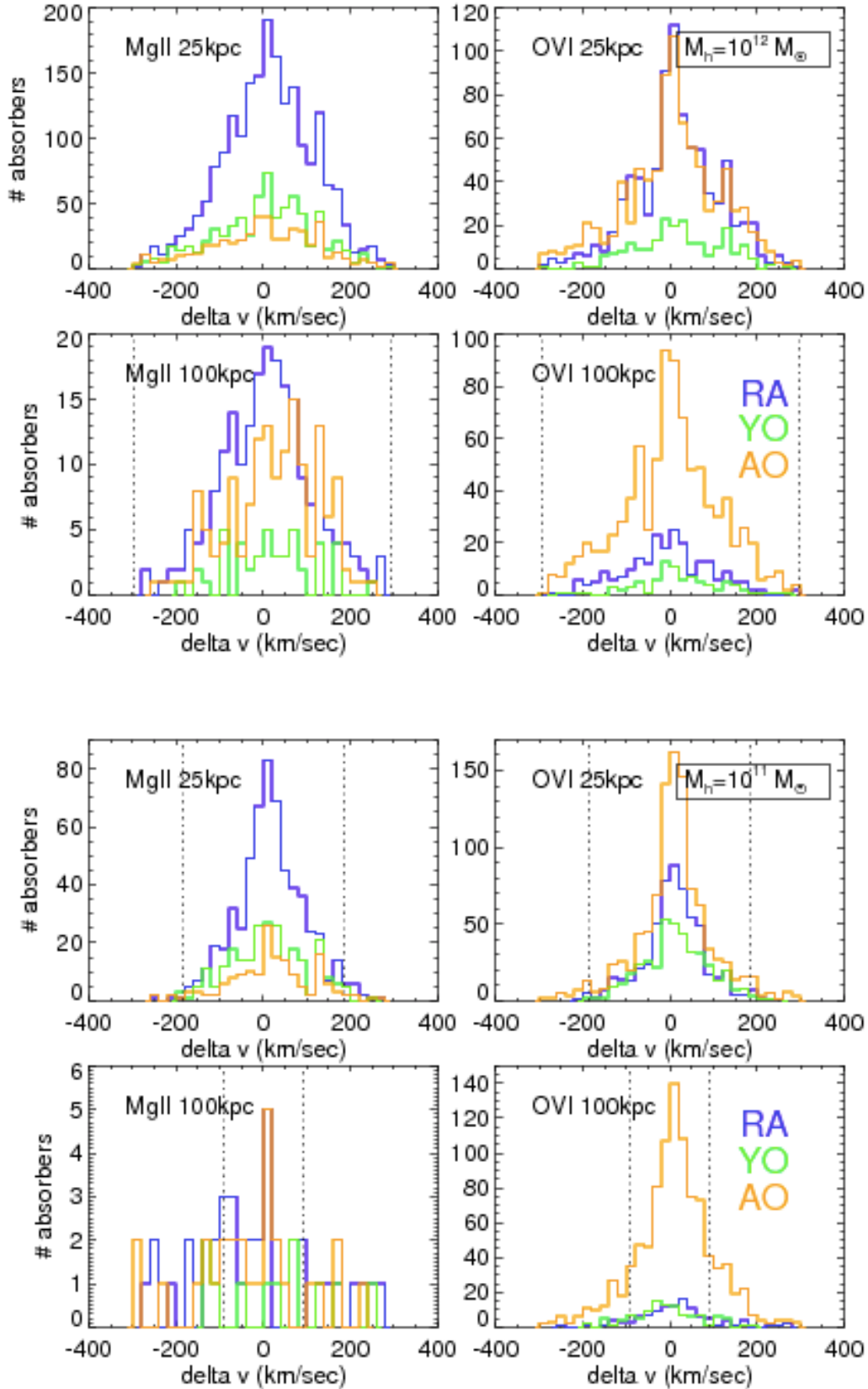
Figure 11. Histograms of velocity, relative to the galaxy systemic velocity, of absorbers split into recycled accretion (blue), young outflows (green), and ancient outflows (orange), for Mg II & O VI, at 25 kpc & 100 kpc as labelled for $10^{12} M_\odot$ (top panels) and $10^{11} M_\odot$ (bottom panels) halos. Vertical lines demarcate the escape velocity at the midpoint of each mass bin for R=25 kpc or 100 kpc as labelled. (Escape velocity for $10^{12} M_\odot$ halos at 25 kpc, 590 km s^{-1}, is outside the range of the plot). Note the different y-axis range for each panel.
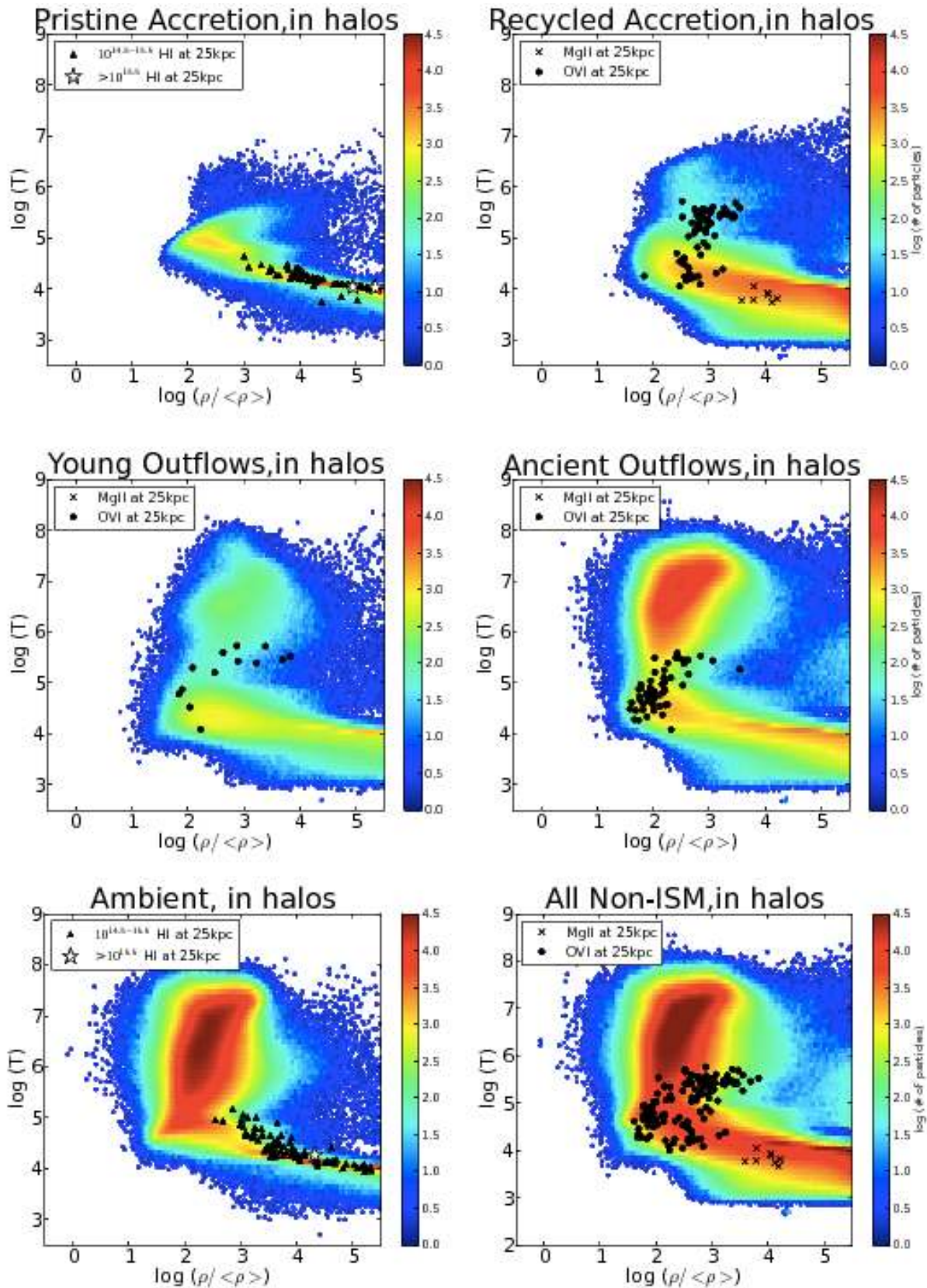
Figure 12. Distribution of gas in temperature-density phase space, for our five categories and for all non-ISM gas, as labelled. We overplot the location of strong ($N > 10^{14}$) absorbers of Mg II and O VI in $10^{12} M_\odot$ halos at 25 kpc, for all non-ISM gas, as well as broken out by category for recycled accretion, young outflows, and ancient outflows. In the pristine accretion and ambient panels, where there is no strong Mg II or O VI absorption in $10^{12} M_\odot$ halos at 25 kpc, we overplot the location of H I absorbers of various strengths as labeled. The colourbar is the same in each panel, showing the log number of particles.
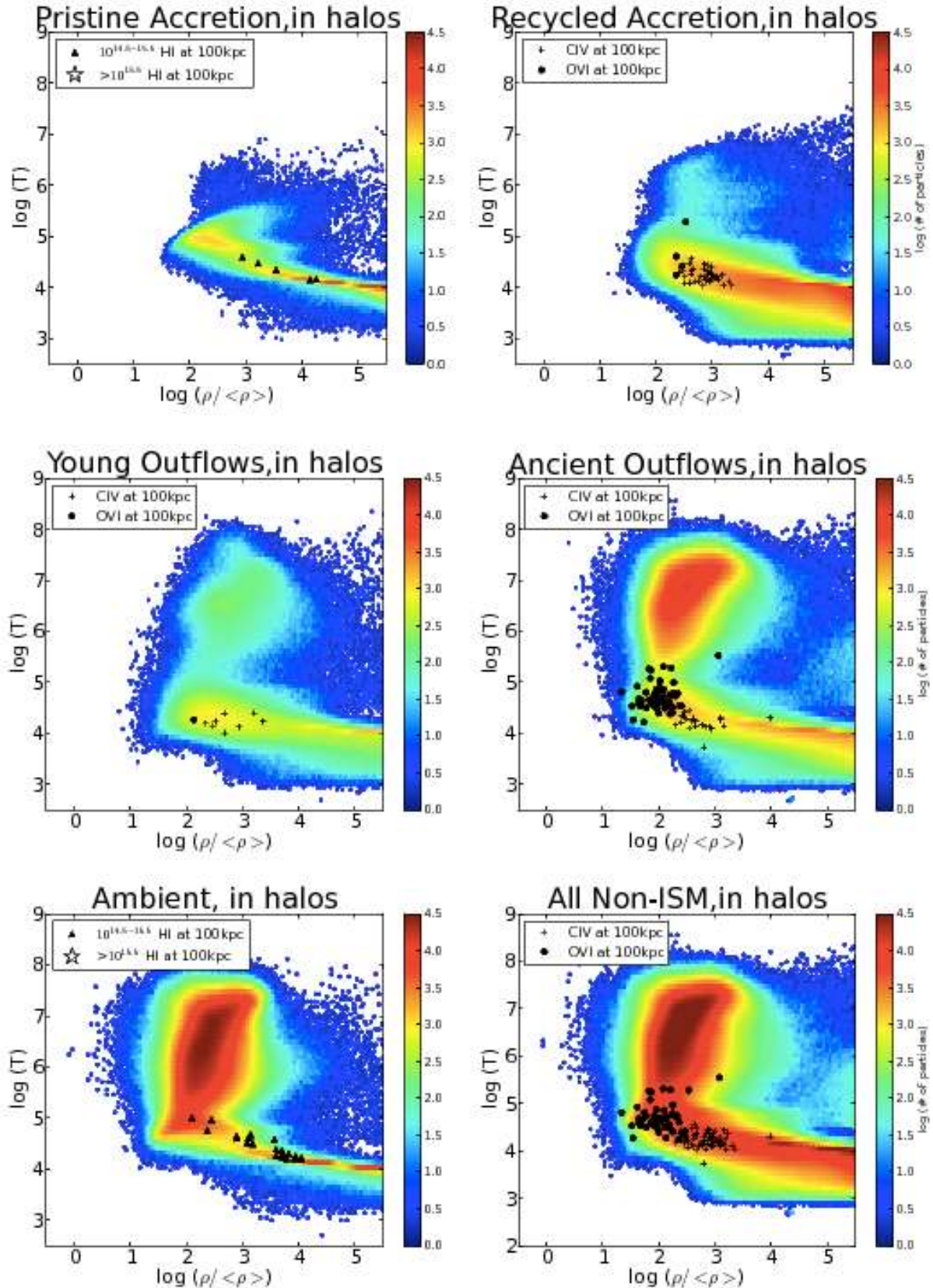
Figure 13. Phase space distributions as in Figure 12. We overplot the location of strong ($N > 10^{14}$) absorbers of C IV and O VI in $10^{12} M_\odot$ halos at 100 kpc, for all non-ISM gas, as well as broken out by category for recycled accretion, young outflows, and ancient outflows. In the pristine accretion and ambient panels, where there is no strong C IV or O VI absorption in $10^{12} M_\odot$ halos at 100 kpc, we overplot the location of H I absorbers of various strengths as labeled. The colourbar is the same in each panel, showing the log number of particles.

collisional ionisation fraction maximum for O VI at around 300,000 K. Therefore, we expect a significant amount of collisionally-ionised oxygen arising in halos, though as we argued in Oppenheimer et al. (2012) and Ford et al. (2013) it is not globally dominant relative to photo-ionised O VI absorption. We emphasize that we have only plotted the strong absorbers here, which for O VI is often collisionally ionised. At 25 kpc there is substantial strong O VI absorption from both recycled accretion and ancient outflows, while at larger impact parameters, it chiefly arises in ancient outflows, (Figure 7 and in Figure 13 below).

Young and ancient outflows (middle panels) are generally at somewhat lower densities, and they show more significant amounts of gas near the virial temperature. Note that in lower mass halos (not shown as a separate subdivision), there is very little of this hotter gas component (e.g. Kereš et al. 2009). O VI absorption still comes from the same general region in these panels as in the recycled accretion panel: warm, low density gas that is both photo-ionised and collisionally-ionised. Although ancient outflows do have some material roughly in the right density/temperature range for strong Mg II absorption, we note that close to galaxies there is very little metal mass in ancient outflows, as shown in Figure 10.

In the lower panels we see even hotter material in the ambient gas (left panel). This material generally has too low a metal content to provide much strong O VI absorption and, furthermore, it has been shock heated to temperatures that are too high for strong Mg II absorption. It is interesting that most of the O VI absorption in our models comes from infalling or (formerly) outflowing gas, not from ambient halo gas. In part this owes to our definition of ambient gas as never having been in an outflow, so it is very difficult for this gas to become enriched. Nonetheless, this indicates that there may be a substantial amount of warm-hot gas within halos that is not traceable via metal lines, and one must rely on, e.g., broad HI absorbers to characterise this gas (e.g. Richter 2012).

In Figure 13 we show the same coloured regions as in Figure 12, but have overplotted absorption at impact parameters of 100 kpc instead of at 25 kpc; at larger impact parameters, ancient outflows dominate the absorption in high ions. Because there is almost no Mg II absorption at 100 kpc, we choose instead to plot C IV with O VI. One can see that O VI comes from warmer, less dense gas, but is rarely collisionally ionized at temperatures $> 10^5$ K. C IV absorption resides at intermediate overdensities between O VI and Mg II as shown in the previous figure.

These plots help answer the question: why is O VI absorption mostly coming from ancient outflows? It is because ancient outflows have more material at the temperatures and densities favourable for O VI formation (and for the formation of high metal ions in general). Conversely, absorption in the low ions largely comes from cold, dense gas that is likely to accrete, so it arises in the recycled accretion category rather than the outflow category. Intermediate ions can have significant contributions from recycled accretion, young outflows, or ancient outflows, depending on the impact parameter.

Moving to HI we see that at 25 kpc (Fig 12) the strong ($N > 10^{14.5}$cm^{-2}) H I absorbers for pristine accretion arise at high densities ($\delta \geqslant 10^3$). In the relation between over-

density and HI column density given by Davé et al. (2010), HI absorbers with $N = 10^{14.5-15.5}$ cm^{-2} are predicted to lie at $\delta = 10^2 - 10^3$, albeit with substantial scatter. Why does pristine accretion not have absorbers in this overdensity range? The absorbers clearly follow the overall peak of the pristine accretion distribution (red/yellow region), and there is simply not enough pristine accretion material in the that overdensity regime to give rise to HI absorption.

This is different from their distribution in the ambient case, where there is strong HI at not only high overdensities, but also at intermediate overdensities of $\delta = 10^2 - 10^3$. This is because there is more mass in ambient material than in pristine accretion material, as shown in Figure 10. The strong absorbers in ambient material can lie at $T > 10^{4.5}$ K, and there is more spread in the temperatures as well: pristine accretion absorbers are all at temperatures $T < 10^5$ K, while some ambient absorbers arise in hotter gas $T > 10^5$ K, though most are from cooler gas. In both pristine accretion and ambient, the very strong ($N > 10^{15.5}$cm^{-2}) absorbers (two for pristine accretion, one for ambient) exist at high overdensities, $> 10^4$, consistent with the relation given by Davé et al. (2010): stronger HI absorption comes from highest density gas, close to galaxies. Note that if we were to display HI absorbers in the recycled accretion panel, there would be significantly more such strong absorbers at these overdensities.

By 100 kpc (Fig. 13), there is much less strong HI and no very strong HI in either category. This is because the overdensity drops with radius, so at larger impact parameter there is less dense material to give rise to HI absorption. There are more absorbers in ambient than in pristine accretion, because at large radius there is more ambient than pristine material, as seen in Figure 10. Like the low/mid metals, HI absorbers generally follow the peak of the gas distribution, excluding areas that are too hot.

Overall, a given metal ion will absorb at similar densities and temperatures across all categories. Whether there is substantial absorption in a given ion from a given category largely depends on how much material in that category lies at the right temperature/density combination for absorption. It is also a function of the total amount of metal mass in a category at a given radius from the galaxy, as discussed in the previous section. Hence in principle, a suite of absorbers spanning a range of ionisation states can probe the full range of physical conditions as a function of radius in the CGM, with the exception of hot unenriched gas.

6 NUMERICAL CONSIDERATIONS

Our predictions depend on both our physical model of galaxy formation and our numerical implementation of that physical model. Key elements of the physical model include the ΛCDM cosmological framework, the adopted cosmological parameter values, standard hydrodynamic and radiative cooling processes, the star formation prescription, and, critically, the ezw wind prescription that sets mass loading factors and ejection speeds. In the absence of winds, different implementations of SPH, adaptive mesh refinement (AMR), and moving mesh hydro simulations show reasonable but not perfect convergence on the mechanisms and rates of galaxy growth. All methods show that halos with $M \lesssim 10^{11.5} M_\odot$

are fed by filaments of cold ($T \sim 10^4\,\mathrm{K}$) gas that penetrate far inside the halo virial radius, and that large halos of shock heated gas (typically $T \gtrsim 10^6\,\mathrm{K}$) develop only at higher halo masses (e.g., Kereš et al. 2005, 2009; Ocvirk et al. 2008; Agertz et al. 2009; Brooks et al. 2009; Ceverino et al. 2010; Nelson et al. 2013). This cold-to-hot transition can be understood analytically in terms of the ratio of gas cooling time to the halo dynamical time (Binney 1977; Rees & Ostriker 1977; Silk 1977; White & Rees 1978; White & Frenk 1991; Birnboim & Dekel 2003; Dekel & Birnboim 2006). In the critical regime near $10^{12} M_\odot$, there is some disagreement among numerical methods on whether cold filaments persist all the way to the central galaxy (Nelson et al. 2013), though this appears to be a shifting of transition boundaries in mass and redshift rather than a universal difference of behaviour.[1] Another significant difference, probably more important for galaxy growth rates, arises in the density profiles and consequent cooling rates of the shock heated gas component. The entropy-based formulation of SPH (Springel & Hernquist 2002) implemented in GADGET-2, and thus in our simulation here, appears to be especially effective at maintaining separation of fluids in different phases and reducing cooling of the hot gas component, relative to other formulations of SPH or to the moving mesh code AREPO (Kereš et al. 2009; Nelson et al. 2013).

While numerical differences of this sort would have some quantitative impact on the kinds of predictions presented here, the more important numerical uncertainties have to do with the implementation of galactic winds themselves. As discussed in §2, we follow Springel & Hernquist (2003) in implementing winds via ejection of particles from the star-forming ISM. Because these wind particles tend to be metal-rich, and because they leave the galaxy at ISM temperatures, they typically have short cooling times and remain cold even when they interact with a surrounding hot halo. Wind particles retain their heavy elements by construction, so there is mixing with the ambient halo gas only to the extent that the particles representing these components become mixed. This behaviour may be a reasonable representation of reality, but it is also possible that instabilities mix wind gas and ambient halo gas on scales below the resolution of our simulation (and perhaps below the resolution of any current cosmological simulations of galaxy formation).

There are strong circumstantial arguments for galactic winds with phenomenology roughly like that of our ezw model, including the low observed ratios of stellar mass to halo baryons, the widespread presence of intergalactic and circumgalactic metals, and direct observations and high-resolution simulations of galaxy outflows. We therefore expect that the global mass and metal budgets in our simulation are approximately correct. However, the detailed density and temperature structure of ejected and recycling gas, and therefore the absorption in individual ionic species, is necessarily more uncertain, and our predictions here should be regarded as specific to our physical model and numerical

implementation of winds. In future work we will use a wind formulation that incorporates an explicit subgrid model for mixing of metals and exchange of thermal energy between wind particles and their neighbours, which will enable us to investigate a range of possible behaviours. Extensive mixing would blur the distinctions between "outflow" gas and "ambient" gas, and between "recycled" and "pristine" accretion, complicating some of the descriptions we have adopted in this paper. More generally, numerical simulations of stellar feedback and the baryon cycle are in a phase of rapid progress, with an increase in the sophistication of models and the range of numerical approaches. We expect that comparison of results from different simulations, and comparison of these results to rapidly improving observations of circumgalactic gas and galactic outflows, will lead to numerous insights and much progress over the next several years.

7   CONCLUSIONS

We examine the physical and dynamical state of gas around galaxies in a $32h^{-1}\mathrm{Mpc}$, quarter-billion particle cosmological hydrodynamic simulation. We concentrate on $z = 0.25$, and use past and future simulation snapshots to delineate which particles have been ejected from galaxies (and how long ago), which particles are falling into galaxies by $z = 0$, whether or not they have previously been part of a galaxy's ISM, and which particles are ambient material not participating in the baryon cycle. We use these categories to examine both observable and physical properties of the gas, to elucidate a connection between observational absorption line probes of the CGM and its dynamical state, i.e. whether it is inflowing, outflowing, or ambient. As in our earlier simulations Oppenheimer et al. (2010), recycled accretion of enriched gas that is ejected in winds and then re-accreted plays a major role in low-redshift galaxy accretion.

Our main findings are as follows:

(i) Most of the absorption of low-ionisation potential metal species owes to enriched material that will fall back into galaxies within a few Gyr. This occurs because low-ionisation species preferentially trace cold, dense, enriched environments, and hydrodynamic interactions generally cannot prevent this gas from accreting.

(ii) Most of the absorption of high-ionisation potential metal species owes to outflows ejected much earlier than the present epoch, "ancient outflows". This occurs because high-ionisation potential species tend to be prominent in warmer, more diffuse environments. Some of this high-ionization material is also re-accreting onto galaxies.

(iii) The metal mass fraction in recycled accretion drops off steeply with R/R_{vir} (see Figure 10), which gives rise to a rapid drop in absorption with impact parameter for low ions. The metal mass in ancient outflows increases mildly with R/R_{vir}, which partly explains why the absorption profile of the high ions stays relatively flat out to the virial radius.

(iv) Low-mass halos ($<10^{11.5}$ $\mathrm{M}_\odot$) have a greater proportion of recycled material than high-mass halos ($>10^{11.5}$ $\mathrm{M}_\odot$). Even though high-mass halos assemble proportionally more of their mass via recycled accretion than pristine accretion (Oppenheimer et al. 2010), recycled accretion represents a proportionally larger fraction of the circumgalactic medium around low-mass halos.

---

[1] For example, the $10^{11.5} M_\odot$ shown by Nelson et al. (2013) at $z = 2$ (their figure 7) looks significantly different between GADGET (SPH) and AREPO (moving mesh), but the $z = 3$ snapshots of the same halo are nearly identical between the two codes (D. Keres 2013, presentation at IAP Colloquium on Origin of the Hubble Sequence).

(v) Where absorption of a given ion is found, that absorption exists at roughly similar densities and temperatures among the various categories. Hence, absorbers with a range of ionisation potentials can broadly trace out the density and temperature structure of the CGM. The strengths of various absorption lines within various inflow/outflow categories primarily reflects the phase space location and metallicity of the gas in those categories.

(vi) HI predominantly traces non-accreting material that has never been in a wind, i.e. "ambient". Ambient material holds the majority of mass in the halo and is quasi-spherical, which is why it dominates the HI absorption and produces a high covering fraction out to the virial radius. There is more strong HI from recycled accretion than pristine accretion.

(vii) Accreting material is not unenriched. Recycled accretion dominates the mass and metal budget of accreting material, and this component is significantly enriched.

(viii) Mg II provides a good tracer of accreting material that was once in a wind ("recycled accretion"). Virtually all strong Mg II absorbers arise in this category of gas. Si IV, despite its high ionisation level, behaves more like Mg II than a high ion.

(ix) C IV represents an intermediate ion. At small impact parameters it mostly arises in recycled accretion, but at larger impact parameters it mostly arises from ancient outflows. The crossover impact parameter is ~ 100 kpc in L^* halos, and moves to smaller impact parameters for smaller halos; for our lowest mass halos, C IV predominantly arises in ancient outflows at all impact parameters.

(x) O VI and Ne VIII almost exclusively trace ancient outflows, at nearly all impact parameters and halo masses (very small impact values around $10^{12} M_\odot$ halos being the exception). A substantial fraction of strong O VI halo absorbers come from transition gas at $\sim 300,000$ K and is cooling out of hot gas near the virial temperature. Photoionised gas at $\sim 10^4$ K also contributes many O VI absorbers, and most of the absorbers at impact parameters $\geqslant 100$ kpc, in agreement with Oppenheimer & Davé (2009).

(xi) In small halos the majority of the accreting mass at $z = 0.25$ is ejected back into a wind by $z = 0$, with only about a quarter of the mass remaining as stars or in the ISM. In larger halos, by $z = 0$ the accreting mass is split evenly between stars, ISM gas, and gas re-ejected as a wind.

(xii) With our definition of accretion (at $z = 0.25$) as any gas that will join a galaxy by $z = 0$, velocity is not very useful for distinguishing accreting gas from outflowing gas. The radial velocity distribution of gas in the recycled accretion, young outflow, and ancient outflow categories is very similar, with the exception that material moving at high outward velocities at small radii does tend to be recently ejected material.

(xiii) Accreting material is not necessarily parallel to the disk, and outflowing material is not necessarily perpendicular to the disk.

(xiv) Of gas not in the ISM at $z = 0.25$, 86% of the mass and 6% of the metal mass has never been in a wind by $z = 0$.

By decomposing our simulated gas distribution into inflows and outflows, we better understand how the material in the CGM by $z = 0.25$ arose, and what its eventual fate is. These results underscore the dynamic nature of the CGM, including how much material is participating in the "baryon cycle", particularly in halo fountains. This means that accreting material is often enriched, and inflows can be traced using metal lines. We emphasize that low ions trace fundamentally different gas (cold, dense, accreting) than high ions (warm, diffuse, from ancient outflows not accreting), and that inflows and outflows have different distributions both in physical and temperature-density phase space. While there is often co-location of gas in various phases giving rise to both low and high ions, it is dangerous to assume that it arises in a single-phase gas. HI has more strong absorption from recycled accretion than pristine accretion, which simply reflects the fact that recycled accretion is dominating the inflow mass budget at low redshifts in our models.

There are clear observational diagnostics amongst ambient material, inflows, and outflows, and even between young ($\leqslant$ Gyr) and ancient ($>$ Gyr) outflows. In general HI traces ambient material, Mg II and Si IV trace recycled accretion, C VI traces both recycled accretion and ancient outflows depending on impact parameter, with O VI and Ne VIII tracing ancient outflows. We also find differences between low ($<10^{11.5}$ M$_\odot$) and high ($>10^{11.5}$ M$_\odot$) mass halos, because high-mass halos suppress infall owing to their higher halo gas temperatures. Assembling these diagnostics into a full census of CGM gas remains a work in progress, but these results can aid in interpreting and understanding absorption-line observations of the CGM.

This paper is the second in a series (Ford et al. 2013, being the first) to confront successful models for galaxy-IGM coevolution with absorption line observations of CGM gas. With direct comparisons to observations from COS soon forthcoming, and ongoing improvements to our simulation methodologies, we hope to answer such questions as "'what is the most realistic description for outflows in simulations?", "what is the phase space structure of the CGM, and how patchy is it?", "how well mixed are the metals?", "what fraction of outflows end up bound to the halo?" and "how tightly are the CGM and its host galaxy linked?". Through these types of investigations, we aim to further constrain our simulations while gaining additional insights into the CGM and the dominant physical processes that impact it.

REFERENCES

Agertz, O., Teyssier, R., & Moore, B. 2009, MNRAS, 397,

L64

—. 2001b, ApJ, 560, 599

Balogh, M. L., Pearce, F. R., Bower, R. G., & Kay, S. T. 2001, MNRAS, 326, 1228

Becker, G. D., Sargent, W. L. W., Rauch, M., & Calverley, A. P. 2011, ApJ, 735, 93

Behroozi, P. S., Wechsler, R. H., & Conroy, C. 2013, ApJ, 770, 57

Berlind, A. A., Weinberg, D. H., Benson, A. J., et al. 2003, ApJ, 593, 1

Binney, J. 1977, ApJ, 215, 483

Birnboim, Y., & Dekel, A. 2003, MNRAS, 345, 349

Bordoloi, R., Lilly, S. J., Knobel, C., et al. 2011, ApJ, 743, 10

Bouché, N., Dekel, A., Genzel, R., et al. 2010, ApJ, 718, 1001

Brook, C. B., Stinson, G., Gibson, B. K., et al. 2012, MNRAS, 419, 771

Brooks, A. M., Governato, F., Quinn, T., Brook, C. B., & Wadsley, J. 2009, ApJ, 694, 396

Ceverino, D., Dekel, A., & Bournaud, F. 2010, MNRAS, 404, 2151

Chabrier, G. 2003, PASP,115, 763

Chen, H.-W. 2012, MNRAS, 427, 1238

Churchill, C. W., Mellon, R. R., Charlton, J. C., et al. 2000, ApJS, 130, 91

Cooksey, K. L., Kao, M. M., Simcoe, R. A., O'Meara, J. M., & Prochaska, J. X. 2013, ApJ, 763, 37

Danovich, M., Dekel, A., Hahn, O., & Teyssier, R. 2012, MNRAS, 422, 1732

D'Odorico, V., Calura, F., Cristiani, S., & Viel, M. 2010, MNRAS, 401, 2715

Davé, R., Hernquist, L., Weinberg, D. H., & Katz, N. 1997, ApJ, 477, 21

Davé, R., Oppenheimer, B. D., Katz, N., Kollmeier, J. A., & Weinberg, D. H. 2010, MNRAS, 408, 2051

Davé, R., Oppenheimer, B. D., & Finlator, K. 2011a, MNRAS, 415, 11

—. 2011b, MNRAS, 416, 1354

Davé, R., Finlator, K., & Oppenheimer, B. D. 2012, MNRAS, 421, 98

Davé, R., Katz, N., Oppenheimer, B. D., Kollmeier, J. A., &Weinberg, D. H. 2013, astro-ph 1302.3631

Dekel, A., & Birnboim, Y. 2006, MNRAS, 368, 2

Dekel, A., Birnboim, Y., Engel, G., et al. 2009, Nature, 457, 451

Erb, D. K., Shapley, A. E., Pettini, M., et al. 2006, ApJ, 644, 813

Faucher-Giguère, C.-A., & Kereš, D. 2011, MNRAS, 412, L118

Ferland, G., Korista, K. T., Verner, D. A., Ferguson, J. W., Kingdon, J. B., Verner, E. M. 1998, PASP, 110, 761

Ford, A. B., Oppenheimer, B. D., Davé, R., Katz, N., Kollmeier, J. A., &Weinberg, D. H. 2013 MNRAS, 432, 89

Fumagalli, M., Prochaska, J. X., Kasen, D., et al. 2011, MNRAS, 418, 1796

Gabor, J. M., & Davé, R. 2012, MNRAS, 427,1816

Genzel, R., Tacconi, L. J., Gracia-Carpio, J., et al. 2010, MNRAS, 407, 2091

Goerdt, T., Dekel, A., Sternberg, A., et al. 2010, MNRAS, 407, 613

Governato, F., Willman, B., Mayer, L., et al. 2007, MNRAS, 374, 1479

Haardt, F., & Madau, P. 2001, in Clusters of Galaxies and the High Redshift Universe Observed in X-rays, ed. D. M. Neumann & J. T. V. Tran

Hinshaw, G., Weiland, J. L., Hill, R. S., et al. 2009, ApJS, 180, 225

Hopkins, P. F., Quataert, E., & Murray, N. 2012, MNRAS, 421, 3522

Hummels, C. B., Bryan, G. L., Smith, B. D., & Turk, M. J. 2013, MNRAS, 430, 1548

Kacprzak, G. G., Churchill, C. W., & Nielsen, N. M. 2012, ApjL, 760, L7

Katz, N., Weinberg, D. H., & Hernquist, L. 1996, ApJS, 105, 19

Kennicutt, Jr., R. C. 1998, ApJ, 498, 541

Kereš, D., Katz, N., Weinberg, D. H., & Davé, R. 2005, MNRAS, 363, 2

Kereš, D., Katz, N., Fardal, M., Davé, R., & Weinberg, D. H. 2009, MNRAS, 395, 160

Kereš, D., & Hernquist, L. 2009, ApjL, 700, L1

Lehner, N., Howk, J. C., Thom, C., et al. 2012, MNRAS, 424, 2896

Lehner, N., Howk, J. C., Tripp, T. M., et al. 2013, ApJ, 770, 138

Martin, C. L. 2005, ApJ, 621, 227

Martin, C. L., Shapley, A. E., Coil, A. L., et al. 2013, ApJ, 770, 41

McKee, C. F., & Ostriker, J. P. 1977, ApJ, 218, 148

Murray, N., Quataert, E., & Thompson, T. A. 2005, ApJ, 618, 569

Murray, N., Quataert, E., & Thompson, T. A. 2010, ApJ, 709, 191

Nelson, D., Vogelsberger, M., Genel, S., et al. 2013, MNRAS, 429, 3353

Ocvirk, P., Pichon, C., & Teyssier, R. 2008, MNRAS, 390, 1326

Oppenheimer, B. D., & Davé, R. 2006, MNRAS, 373, 1265

Oppenheimer, B. D., & Davé, R. 2008, MNRAS, 387, 577

—. 2009, MNRAS, 395, 1875

Oppenheimer, B. D., Davé, R., Kereš, D., et al. 2010, MNRAS, 406, 2325

Oppenheimer, B. D., Davé, R., Katz, N., Kollmeier, J. A., & Weinberg, D. H. 2012, MNRAS, 420, 829

Pettini, M., Shapley, A. E., Steidel, C. C., et al. 2001, ApJ, 554, 981

Prochaska, J. X., Hennawi, J. F., & Simcoe, R. A. 2013, ApjL, 762, L19

Rees, M. J., & Ostriker, J. P. 1977, MNRAS, 179, 541

Richter, P. 2012, ApJ, 750, 165

Rubin, K. H. R., Prochaska, J. X., Koo, D. C., & Phillips, A. C. 2012, ApJL, 747, L26

Rudie, G. C., Steidel, C. C., Trainor, R. F., et al. 2012, ApJ, 750, 67

Rudie, G. C., Steidel, C. C., Shapley, A. E., & Pettini, M. 2013, ApJ, 769, 146

Rupke, D. S., Veilleux, S., & Sanders, D. B. 2005, ApJ, 632, 751

Schmidt, M. 1959, ApJ, 129, 243

Silk, J. 1977, ApJ, 211, 638

Simcoe, R. A., Cooksey, K. L., Matejek, M., et al. 2011, ApJ, 743, 21

Songaila, A. 2001, ApjL, 561, L153

Springel, V., & Hernquist, L. 2002, MNRAS, 333, 649

—. 2003, MNRAS, 339, 289

Springel, V. 2005, MNRAS, 364, 1105

< Steidel, C. C. 2001, in Bulletin of the American Astronomical Society, Vol. 33, American Astronomical Society Meeting Abstracts #198, 863

Steidel, C. C., Erb, D. K., Shapley, A. E., et al. 2010, ApJ, 717, 289

Stinson, G. S., Brook, C., Prochaska, J. X., et al. 2012, MNRAS, 425, 1270

Stocke, J. T., Keeney, B. A., Danforth, C. W., et al. 2013, ApJ, 763, 148

Tacconi, L. J., Genzel, R., Neri, R., et al. 2010, Nature, 463, 781

Thom, C., & Chen, H.-W. 2008, ApJS, 179, 37

Thom, C., Tumlinson, J., Werk, J. K., et al. 2012, ApjL, 758, L41

Tilton, E. M., Danforth, C. W., Shull, J. M., & Ross, T. L. 2012, ApJ, 759, 112

Torrey, P., Vogelsberger, M., Genel, S., et al. 2013, ArXiv e-prints

Tremonti, C. A., Moustakas, J., & Diamond-Stanic, A. M. 2007, ApJL, 663, L77

Tripp, T. M., Savage, B. D., & Jenkins, E. B. 2000, ApJL, 534, L1

Tripp, T. M., Aracil, B., Bowen, D. V., & Jenkins, E. B. 2006, ApJL, 643, L77

Tripp, T. M., Sembach, K. R., Bowen, D. V., et al. 2008, ApJS, 177, 39

Tripp, T. M., Meiring, J. D., Prochaska, J. X., et al. 2011, Science, 334, 952

Tumlinson, J., Thom, C., Werk, J. K., et al. 2011, Science, 334, 948

Tumlinson, J., Thom, C., Werk, J. K., et al. 2013, ApJ, accepted

van de Voort, F., Schaye, J., Altay, G., & Theuns, T. 2012, MNRAS, 421, 2809

Veilleux, S., Cecil, G., & Bland-Hawthorn, J. 2005, ARAA, 43, 769

Weiner, B. J. 2009, in American Institute of Physics Conference Series, Vol. 1201, American Institute of Physics Conference Series, ed. S. Heinz & E. Wilcots, 142–145

Werk, J. K., Prochaska, J. X., Thom, C., et al. 2013, ApJS, 204, 17

White, S. D. M., & Rees, M. J. 1978, MNRAS, 183, 341

White, S. D. M., & Frenk, C. S. 1991, ApJ, 379, 52

Wiersma, R. P. C., Schaye, J., & Smith, B. D. 2009a, MNRAS, 393, 99

Wiersma, R. P. C., Schaye, J., Dalla Vecchia, C., et al. 2010, MNRAS, 409, 132